SCIENCE CHINA
Earth Sciences

•RESEARCH PAPER•

https://doi.org/10.1007/s11430-022-1008-5

Flood variability in the upper Yangtze River over the last millennium—Insights from a comparison of climate-hydrological model simulated and reconstruction

Ran HUO[1,2], Hua CHEN[1,2*], Lu LI[3], Chong-Yu XU[4,1*†], Jingjing LI[1], Si HONG[1], Chesheng ZHAN[5] & Jun XIA[1,6]

[1] *State Key Laboratory of Water Resources and Hydropower Engineering Science, Wuhan University, Wuhan 430072, China;*
[2] *Hubei Provincial Key Lab of Water System Science for Sponge City Construction, Wuhan University, Wuhan 430072, China;*
[3] *NORCE Norwegian Research Centre, Bjerknes Centre for Climate Research, Jahnebakken 5, 5007 Bergen, Norway;*
[4] *Department of Geosciences, University of Oslo, P.O Box 1047 Blindern, 0316 Oslo, Norway;*
[5] *Key Laboratory of Ecosystem Network Observation and Modeling, Institute of Geographic Sciences and Natural Resources Research, Chinese Academy of Sciences, Beijing 100101, China;*
[6] *Key Laboratory of Water Cycle and Related and Surface Processes, Chinese Academy of Sciences, Beijing 100101, China*

Received March 2, 2022; revised August 27, 2022; accepted September 15, 2022; published online January 19, 2023

Abstract Understanding hydrological responses to rising levels of greenhouse gases are essential for climate and impact research. It is, however, often limited by a lack of long record of observational data to provide a basis for understanding the long-term behavior of the climate system. Integrating reconstructed data and (global climate and hydrological) model simulations will help us to better understand the variability of climate and hydrology over timescales ranging from decades to centuries. In this study, we proposed an integrated approach to study flood variability in the upper reach of the Yangtze River over the last millennium to the end of the 21st century. To accomplish this, we first drove hydrological models using the precipitation and temperature from four Global Climate Models (GCM), BCC-CSM1.1, MIROC, MRI-CGCM3, and CCSM4, to simulate daily discharge for the upper reach of the Yangtze River during the period of the last millennium (850–1849), historical period (1850–2005), and a future period (2006–2099). Then, we evaluated whether the modeled precipitation, temperature, and extreme discharge had statistical properties similar to those shown in the documented dry-wet periods, temperature anomalies, and paleoflood records. Finally, we explored the extreme discharge variability using model simulations. The results indicate that: (1) The MIROC-ESM model, differing from the other three GCM models, revealed positive temperature changes from the warm period (Medieval Climate Anomaly; MCA) to the cold period (Little Ice Age; LIA), while the temperature variability of the other models was similar to the records. (2) The BCC-CSM1.1 model performed better than the others regarding correlations between modeled precipitation and documented dry-wet periods. (3) Over most of the subbasins in the upper Yangtze River, the magnitude of extreme discharge in the BCC-CSM1.1 model results showed that there was a decrease from the MCA to the LIA period and an increase in the historical period relative to the cold period, while a future increase was projected by the four GCMs under the influence of climate change.

Keywords Climate change, Flood variability, Paleoflood records, Climate-hydrological model, Upper Yangtze River

Citation: Huo R, Chen H, Li L, Xu C Y, Li J, Hong S, Zhan C, Xia J. 2023. Flood variability in the upper Yangtze River over the last millennium—Insights from a comparison of climate-hydrological model simulated and reconstruction. Science China Earth Sciences, 66, https://doi.org/10.1007/s11430-022-1008-5

* Corresponding author (email: chua@whu.edu.cn)
† Corresponding author (email: c.y.xu@geo.uio.no)

1. Introduction

Climate warming has led to increased extreme events, including heavy precipitation and river floods, due to higher water-holding capacity in a warmer atmosphere. Floods are one of the most common natural disasters on earth. The economic costs of hazardous flood events are increasing in many parts of the world, including China, and this trend is likely to intensify in the coming decades (Tian, 2015; Li et al., 2022). Most importantly, the space-time distributions of floods are changing both in terms of magnitude and frequency, motivating us to study new methods that not only link diverse types of data but also link flood information on different time scales (Viglione et al., 2013). These events have stimulated a number of scientific studies about proxy-based reconstructions, which provide useful insights into hydrological processes and flood variability longer than the instrumental record (Xiao et al., 2016; Xu et al., 2020).

A great deal of previous research has focused on using river or lake sediment archives and/or records from historical documents to infer the variability of floods over a longer period than conventional observations. A recent study by Engeland et al. (2020) analyzed sediments extracted from Lake Flyginnsjøen in Norway, including high-resolution X-ray, magnetic susceptibility, and CT scans, and used these data to estimate the flood frequency at Elverum station over the past 10,300 years. Munoz et al. (2018) reconstructed flood peak and flood frequency over the past 500 years (1500–2000) based on lake sediments in the lower Mississippi River and tree ring records and found that the 100-year flood increased by 20% over the past five centuries. Paleoflood slackwater deposits were found along the upper-reach gorges of the Hanjiang River (Li, 2014; Zha et al., 2017). They obtained a series of Holocene flood events for a 10,000-year timescale at the catchment scale through observations and laboratory analyses, which is important for understanding the regional hydrological responses to climate change. More recently, an analysis of extreme floods in the Yangtze River over the past millennium was performed by Zhou et al. (2021). A sediment core from the subaqueous delta of the Yangtze River was used to establish a flood history during the last Holocene, revealing 14 multidecadal periods of extreme floods. The results showed a strong influence of the Asian summer monsoon and ENSO on major flood events and the increasing flood frequency over the past 600 years. In addition, historical documents also provide important records to further illuminate the long-term evolution of flood events. For example, Tang and Feng (2021) used 365 extreme events reported in the literature related to floods and droughts to reconstruct a series of flood and drought events for the Hexi Corridor from 0 to 1950 AD. Similar studies were performed by Zhang et al. (2007) and Li et al. (2020) for the Yangtze River and Yellow River based on historical river floods. The developed flood frequency records provided an opportunity to investigate the river's long-term flood dynamics.

There is no doubt that reconstructed floods play a vital role in revealing the statistical characteristics of past climate. However, paleoclimate and paleoflood records with sufficient length and temporal resolution are often scarce in many areas (Lewis, 2018). In addition, sedimentary records are affected by floods of different magnitudes and frequencies, leaving a huge challenge to accurately distinguish floods of different sizes and quantify the magnitude and frequency of paleofloods when using only sedimentary records and/or historical records (Smith et al., 2010). Numerical modeling provides a crucial complementary method for understanding flood event characteristics for those periods without instrumental records. For example, Xu (2015) investigated the water and sediment discharge variations in the Poyang Lake basin (subbasin of the Yangtze River) over the last 1,000 years using the climate model output and the HYDROTREND hydrological model, and the study found that during the period of 1000–2000, climate change was the dominant factor for water discharge variations, but human activity was responsible for the sediment load variations that contributed to Poyang Lake. Recently, Sheng et al. (2020) used the ECHO-G climate model and hydrological model to reconstruct daily discharge and analyze the variability of extreme discharges of the Yalu River for the 1000–2012 period. They found that the frequency curve of extreme discharge events from 1451 to 1850 is similar to that from 1000 to 1450. However, due to climate changes and human activities, there was a 10.47% increase in the frequency of extreme discharge events from 1840 to 2012. To explore the drivers of floods in the Mississippi River, van der Wiel et al. (2018) used a global climate model coupled with surface water modules to simulate extreme discharge in a pre-industrial climate of 3,400 years, and the potential change in future extreme hydrological events due to global warming was also discussed. The results indicated that the coupled land-atmosphere system model provides a mechanism for studying flood events under different climatic conditions. Some have used the climate of the last interglacial period (LIG; 129 to 116 kyr. ago) to analogize a warming future owing to similarities in geological time and temperature. Scussolini et al. (2020) utilized climate models, the PCR-GLOBWB hydrological model, and the CaMa-Flood hydrodynamic model to simulate LIG discharge and 100-yr floods.

The traditional approach to analyzing paleofloods is to use riverine or lacustrine sedimentological records and/or historical documents to infer the flood events (flood occurrence time and flood peak discharge) during the past 1,000 years. Currently, some scholars have used mathematical methods to simulate long-term runoff processes and floods. The Coupled

Model Intercomparison Project Phase 5 (CMIP5) models provide a time series of climate variables for the last millennium (850–1849) (Taylor et al., 2012), which is identified as two significantly different climate periods in the past 1,000 years in the reconstructed paleoclimate. Specifically, there is a warm period called the Medieval Climate Anomaly (MCA) and a cold period called the Little Ice Age (LIA), which are considered to be the warm and cold periods closest to modern times (Wang, 2010). And it is recognized as natural climate variability because it occurred before the age of modern warming. Thus, over the past 1,000 years, there has been a warm and cold climatic transition, which provides an opportunity to investigate the response of floods to climate change and the relationship between climate and hydrology (floods).

The main goal of the study was to explore changes in climate and hydrological extremes on a decadal time scale in the upper Yangtze River Basin using a model chain method consisting of a hydrological model, bias-correction method, and an ensemble of GCMs. To achieve the overall goal, the following subobjectives were accomplished: (1) We conducted a simulation of daily discharges into the various subbasins of the upper Yangtze River Basin for the last millennium using a model chain method and comparison of modeled flood events with paleoflood records; (2) We evaluated the similarities and differences in local hydrological extremes and variations over the last millennium driven by different GCMs; and (3) We investigated the variability of climate and hydrological extremes over the last millennium to the end of the 21st century for the upper Yangtze River Basin.

2. Study area and data

The upper reach of the Yangtze River extends from its source to the Yichang hydrological station in Hubei Province through the Qinghai, Xizang, Sichuan, Yunnan, Chongqing, and Hubei provincial-level regions (Figure 1). The study region is 4,504 km in length and has a total basin area of approximately 1 million km^2 (Gao et al., 2012). The average annual temperature was 12.7°C, and the average annual precipitation was approximately 859 mm during the period of 1955–2011 (Chen et al., 2014). Precipitation is mainly concentrated from late spring to mid-autumn, with a cold-dry winter and a hot-wet summer.

The main tributaries of the upper reach of the Yangtze River are Jinshajiang River, Minjiang River, Tuojiang River, Jialing River, and Wujiang River (Figure 1), with significant vertical drop torrents and many gorges (Gao et al., 2012). In this study, seven subbasins are included in the analysis. The Jinshajiang River is divided into two subbasins: the basin above Shigu station is located in the longitudinal valley with precipitation below 600 mm yr^{-1}. Precipitation increases in the basin below Shigu station, and the average value above Pingshan station is approximately 800 mm yr^{-1}, accounting for approximately one-third of the total runoff above Yichang station. The control hydrological station of the Minjiang River is Gaochang Station 29 kilometers from the river mouth, with annual precipitation varying from 600 to 1,300 mm yr^{-1} for the whole basin. The average annual temperature of the Tuojiang River (Funshun station as outlet) is 17.1°C, and the precipitation is concentrated from June to September, accounting for approximately 70% of the annual precipitation. The Jialing River Basin is the largest subbasin in the tributaries of the upper Yangtze River, with Beibei station as the outlet. The Wujiang River is the largest tributary of the southern bank of the upper Yangtze River Basin, and Wulong serves as a control hydrological station.

The observed daily precipitation and temperature data from 70 meteorological stations (1961–2005) in or around the study area were provided by the China Meteorological Data Service Center. Daily discharge data (1961–2005) from seven hydrological stations were obtained from the Yangtze River Hydrological Bureau of China. In addition, we collected the paleoflood records of Yichang station (Ge, 2009), all of which caused substantial economic losses and fatalities (see Table 1 for more detailed information). The main paleoflood records, including flood peaks and years, have been determined according to the inscriptions of flood marks and historical documents.

For climate model data, newly released data were made available from CMIP6 since 2019; however, only the MRI-ESM2.0 model is available from CMIP6 GCMs for daily precipitation and temperature during the period of 850–2099 (https://esgf-node.llnl.gov/search/cmip6/). Four GCMs (e.g., BCC-CSM1.1, MIROC-ESM, MRI-CGCM3, and CCSM4) from CMIP5 GCMs have daily precipitation and temperature during the last millennium to the end of the 21st century with different future scenarios, which are collectively used in the study. We obtained daily precipitation and temperature data over the last millennium period (850–1849, past 1000), historical period (1850–2005, historical), and future period (2006–2099) under two RCP scenarios (RCP2.6 and RCP8.5) (see Table 2). More details on the design of the CMIP5 experiments can be found in the previous study by Huo et al. (2021).

3. Methods

3.1 Hydrological model

The Xinanjiang (XAJ) model was developed by Professor Zhao Renjun and his team at Hohai University in the 1970s based on the concept of the saturation excess runoff generation mechanism (Zhao, 1992), which has since been

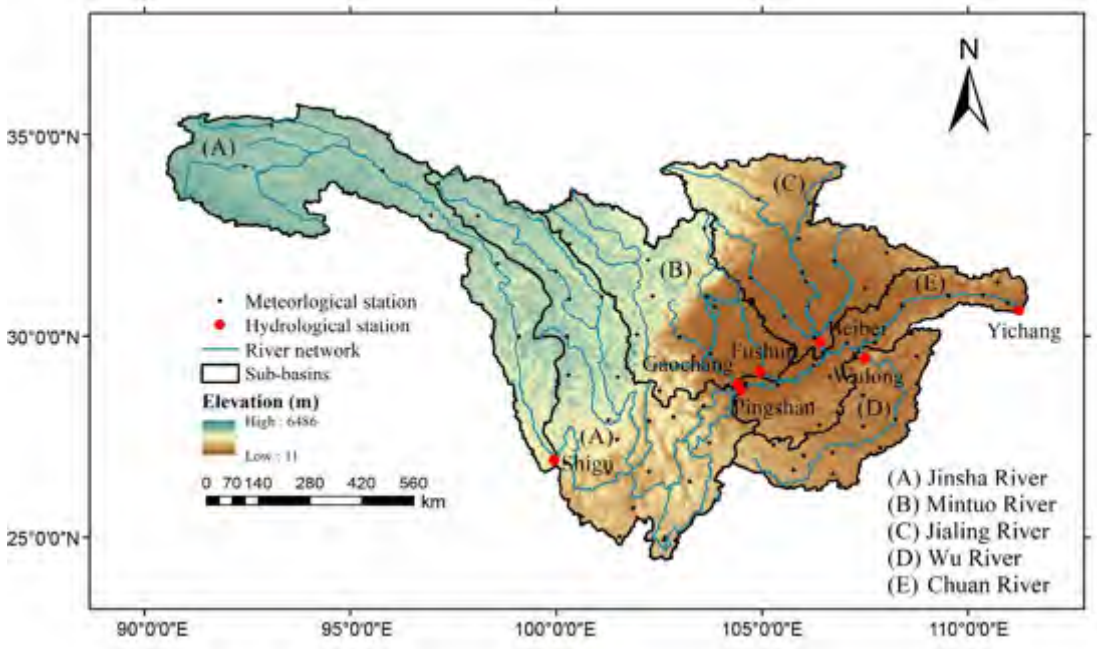

Figure 1 Topography and river networks of the upper reach of the Yangtze River, including hydrological stations of subbasins and meteorological stations.

widely applied in humid and semihumid areas worldwide for hydrological simulation with good performance (Zeng et al., 2016; Yang et al., 2020). The general structure of the XAJ model consists of four units: evapotranspiration calculation, runoff production, separation of runoff components, and flow routing.

In this study, odd years and even years of 1961–2005 were used for calibration and validation, respectively, to minimize the effect of potential changes in climate and land use on model parameters and to maintain consistent conditions in the calibration and validation periods. The model parameters were calibrated using daily observed discharge data from each outlet of the subbasin. The shuffled complex evolution algorithm (SCE-UA) was applied for model calibration, and the Nash-Sutcliffe coefficient (NSE) was used as the objective function (Nash and Sutcliffe, 1970; Dong et al., 2012). Then, the calibrated parameters were used to simulate the long-term runoff series of 1,250 years in the upper reach of the Yangtze River. According to the watershed topography and location of hydrological stations, the feature extraction of the digital basin based on a digital elevation model (DEM) was adopted to divide the subbasins (Figure 1). There are seven subbasins, including the Shigu and Pingshan basins in the Jinshajiang River, the Gaochang and Fushun basins in the Mintuo River, the Beibei basin in the Jialing River, the Wulong basin in the Wu River, and the Yichang basin located along the mainstream of the Yangtze River. The calibrated XAJ model was established in each independent subbasin, and the runoff concentration of the main river (Yichang station) was obtained using the Muskingen routing method.

3.2 Bias-correction method

The daily bias correction (DBC) method proposed by Chen et al. (2013) was used in this study, which is a combination of the DT (daily translation) method and LOCI (local intensity scaling) method, and simultaneously considers deviations of precipitation amount and occurrence frequency.

This method contains two steps: (1) Precipitation frequency is corrected through the LOCI method. Daily precipitation over 0 mm for observations is regarded as a rainy day to determine the occurrence frequency of observed precipitation. Thus, a wet-day threshold in the GCM daily precipitation sequences is determined for each month according to the frequency of observed values. (2) The DT method is used to achieve the correction of each quantile of GCM variables, which is based on the frequency distribution of observed precipitation/temperature series. The formulas are as follows:

$$P_{\text{cor, past/fut, }d} = P_{\text{GCM, past/fut, }d} \times \left(\frac{P_{\text{obs, perc}}}{P_{\text{ref, perc}}}\right), \tag{1}$$

$$T_{\text{cor, past/fut, }d} = T_{\text{GCM, past/fut, }d} + \left(T_{\text{obs, perc}} - T_{\text{ref, perc}}\right), \tag{2}$$

where $P_{\text{cor, past/fut, }d}$ and $P_{\text{GCM, past/fut, }d}$ represent the corrected and original GCM precipitation for Day d in the past 1000 or future period (unit: mm), respectively; $P_{\text{obs, perc}}$ and $P_{\text{ref, perc}}$ represent the daily observed and original GCM precipitation (unit: mm), respectively, for the reference period for the specified percentile perc. In addition, T is the air temperature.

Table 1 Information about large paleofloods at Yichang station

Year	Information
1153	From the upstream of Mintuo river and the downstream of Jialing River, which was the earliest recorded flood. The peak discharge of the Yichang station was estimated to be 94,000 $m^3 s^{-1}$, and the water level was 58.06 m.
1227	From the Chuan River, which was a regional flood. The peak discharge of Yichang station reached 96300 $m^3 s^{-1}$, which was prominent in the historical floods of the upper reach of the Yangtze River.
1560	The main rain areas were in the lower section of Jinshajiang River, Fu River (a tributary of the Jialing River), Jialing River, and Three Gorges region (from the east of Chongqing to Yichang). Pingshan county was flooded. The peak discharge of the Yichang station was estimated to be 98000 $m^3 s^{-1}$, and the water level was 58.45 m.
1613	The peak discharge of Yichang station was estimated to be 81000 $m^3 s^{-1}$
1788	Floods occurred in the upper, middle, and lower reaches of the Yangtze River in 1788. The flood was characterized by the early flood season (April to May). From June to July, the precipitation intensity was large, and the range was wide, which caused floods in Mintuo and Fu rivers. Heavy rain of the Three Gorges region resulted in a huge flood peak of 86,000 $m^3 s^{-1}$ in Yichang station.
1796	Mainly from the Jialing River and Three Gorges region. The peak discharge of the Yichang station was estimated to be 84,000 $m^3 s^{-1}$, and the water level was 56.81 m.
1860	The peak discharge in Yichang station reached 92,500 $m^3 s^{-1}$ on July 18, causing widespread flooding in the upper and middle reaches of the Yangtze River and the Dongting Lake area.
1870	This was the largest flood in the upper and middle reaches of the Yangtze River in more than 800 years since 1153, which was formed by long-lasting, heavy rainfall. The highest water level of Yichang station was 59.50 m, and the peak discharge was 105,000m^3/s, which is four times the annual average discharge of the Yangtze River.
1896	The peak discharge of Yichang station was estimated to be 71,000 $m^3 s^{-1}$
1931	Two heavy rains in August caused flooding on the upper reach of the Yangtze River. In addition, the peak discharge of the Yichang flood was 64,800 $m^3 s^{-1}$ on August 10.
1945	The peak discharge was 67,500 $m^3 s^{-1}$ at Yichang station.
1954	Continuous heavy in the upper reach of the Yangtze River has caused a rare flood in Yichang. From July 7 to August 7, four flood peaks occurred consecutively within a month, the highest water level was 55.73 m, and the corresponding flood peak flow was 66,800 $m^3 s^{-1}$.
1981	In the early morning of July 17, the largest flood peak of the mainstream of the Yangtze River since 1949 reached Gezhouba. The water level of the Yichang station was 55.38 m, and the peak discharge was 70,800 $m^3 s^{-1}$.
1998	The peak discharge was 66,300 $m^3 s^{-1}$ at Yichang station.

Table 2 Main information for global climate models

Model name	Modeling group	Resolution (Lat×Lon)
BCC-CSM1.1	Beijing Climate Center, China Meteorological Administration, China	2.8°×2.8°
MIROC-ESM	Atmosphere and Ocean Research Institute (The University of Tokyo), National Institute for Environmental Studies, and Japan Agency for Marine-Earth Science and Technology, Japan	2.8°×2.8°
MRI-CGCM3	Meteorological Research Institute, Japan	1.125°×1.125°
CCSM4	National Center for Atmospheric Research, US DOE/NSF, USA	0.9°×1.25°

To evaluate the suitability of the bias-correction method, the DBC method was calibrated to areal observations (precipitation and temperature) for each basin for the historical period of 1961–1985 and validated for the period of 1986–2005. We used the two-sample Kolmogorov-Smirnov (KS) test, a nonparametric method, to evaluate the difference in the cumulative distributions (CDFs) between the original/corrected GCM and observations for the calibration and validation periods (Tschöke et al., 2017). In this test, indices of precipitation/temperature were compared between original/corrected GCM and observed data for the KS test (at the 5% significance level), and the null hypothesis (H0) is that they are from the same continuous distribution, whereas the alternate hypothesis (H1) is that they are from different continuous distributions. Specifically, the larger the statistic is, the greater the distribution difference between the observed and GCM output. Finally, a longer time series covering 1961–2005 was used to calibrate the DBC method, and the calibrated bias-correction model was applied to obtain past and future climate data, including precipitation and temperature.

3.3 Anomaly analysis

3.3.1 Precipitation and temperature anomalies

An anomaly analysis was applied to show the evolution of projected precipitation and temperature from four GCMs, which are averaged spatially over each subbasin of the upper reach of the Yangtze River and temporally during the period of 850–2099 (Huang et al., 2013). For this analysis, the observed area-averaged annual precipitation, maximum 1-day precipitation, and mean temperature of 1971–2000 was

calculated as the baseline values. Then, these anomalies were presented in terms of percentage changes of simulated area-averaged indicators from the GCMs for the period 850–2099 relative to baseline values. In addition, the 30-year moving average method was also used to reduce the fluctuation of long series data and clearly see the variation in precipitation and temperature.

$$A_p = \frac{S_p - \overline{O_p}}{O_P}, \tag{3}$$

where A_p, S_p / O_P and $\overline{O_p}$ are the precipitation/temperature anomaly, the simulated/observed area-averaged precipitation/temperature indices, and the baseline value, respectively.

3.3.2 Precipitation frequency anomalies

To evaluate the corresponding relation between GCM precipitation and documented dry-wet periods, we calculated the frequency anomalies for annual precipitation and precipitation in the flood season over the last millennium. The frequency anomalies are calculated in two steps: (1) first, we rank the annual indicators from highest to lowest and calculate the frequency ranging from 0 to 1; (2) anomalies are calculated as frequency values minus 0.5. Therefore, the negative/positive frequency anomalies (negative values of the *y*-axis) indicate larger/smaller precipitation events. Then, the proportions of frequency anomalies less than 0 in each period are also counted. In our study, we consider a model-simulated wet and dry period to be a specific period with a percentage of negative anomaly values larger than or equal to 50% and smaller than 50%, respectively.

3.4 Period division

We compared the lower- and upper-quantile values for the annual maximum 1-day discharge in each subbasin for various experiments. Because the past (1,000-year) simulations are substantially longer than historical (156-year) and future RCP scenarios (94-year), the same number of modeled samples from four experiments should be chosen to maintain consistency. In this case, the historical period of 1912–2005 was first selected, which is the same length as the future period. In addition, the past 1,000 years were divided into the MCA and LIA periods from the paleoclimatic reconstructions. In general, China is divided into five regions based on geographic location, including Northeast, Central-East, Southeast, Northwest, and Qinghai-Xizang Plateau (Ge et al., 2010, 2013, 2017). The Qinghai-Xizang plus (87°–102° E,27°–38°N) the Central-East China (East of 105°E, 25°–38°N) regions cover the whole area of the upper Yangtze River basin. Previous studies show that the reconstructed temperature anomalies of Eastern Qinghai-Xizang Plateau and Central-East China are somewhat different for the LIA period. A larger temperature change is found in Central-East China, while a smaller change is found in the Eastern Qinghai-Xizang Plateau. In this study, we selected the period of 1400–1849, a wider time range, as cold period (Wang and Wang, 1991; Ge et al., 2017) considering the relatively smaller temperature changes during 1550–1850 and a temperature decline from 1400 to 1550 in the Eastern Qinghai-Xizang Plateau. Hence, we choose the periods of 900–1200 and 1400–1849 as warm periods in the MCA and cold periods in the LIA, respectively. A bootstrap method was applied to obtain samples for the 900–1200 and 1400–1849 periods for the maximum 1-day discharge data of the last millennium. The bootstrap method (Hinkley, 1988) is a uniform resampling technique with replacement. The dataset is sampled *m* times with replacement to generate a set of *m* samples. In this way, some samples in the original data sample are likely to appear multiple times in the sample set. Specifically, 10,000 time series of 94-year length were synthesized for the periods of 900–1200 and 1400–1849, and quantiles were calculated for each synthesis. Then, a median value of the bootstrapped data was calculated for each quantile.

4. Results

4.1 Evaluations

4.1.1 Hydrological evaluation of the XAJ model

The performances of the XAJ model for the main hydrologic stations in the upper reach of the Yangtze River are presented in Figure 2, which shows that the XAJ model can effectively capture the same seasonal pattern and the dynamics of the hydrographs at the main hydrologic stations. The average NSE values for the XAJ model are 0.84 and 0.83 for the calibration and validation periods, respectively, indicating the reliable performance of the model in the study basins. The Yichang station is the control station of the mainstream of the upper reach of the Yangtze River, including upstream discharge from the Pingshan, Gaochang, Fushun, Beibei, and Wulong stations. The discharge hydrographs of Yichang indicate good performance of XAJ in simulating the discharge of the upper Yangtze River Basin directly (red line) at the mainstream station or separately (blue line) at sub-basin stations (Figure 2g).

4.1.2 Calibration and validation of precipitation and temperature from the DBC method

The performance of the DBC method for the bias-corrected precipitation and temperature was evaluated using the KS test to check the difference in the cumulative distribution between the original GCMs and corrected GCM data. We calculated areal indices, including annual precipitation, maximum 1-day precipitation, and annual mean temperature,

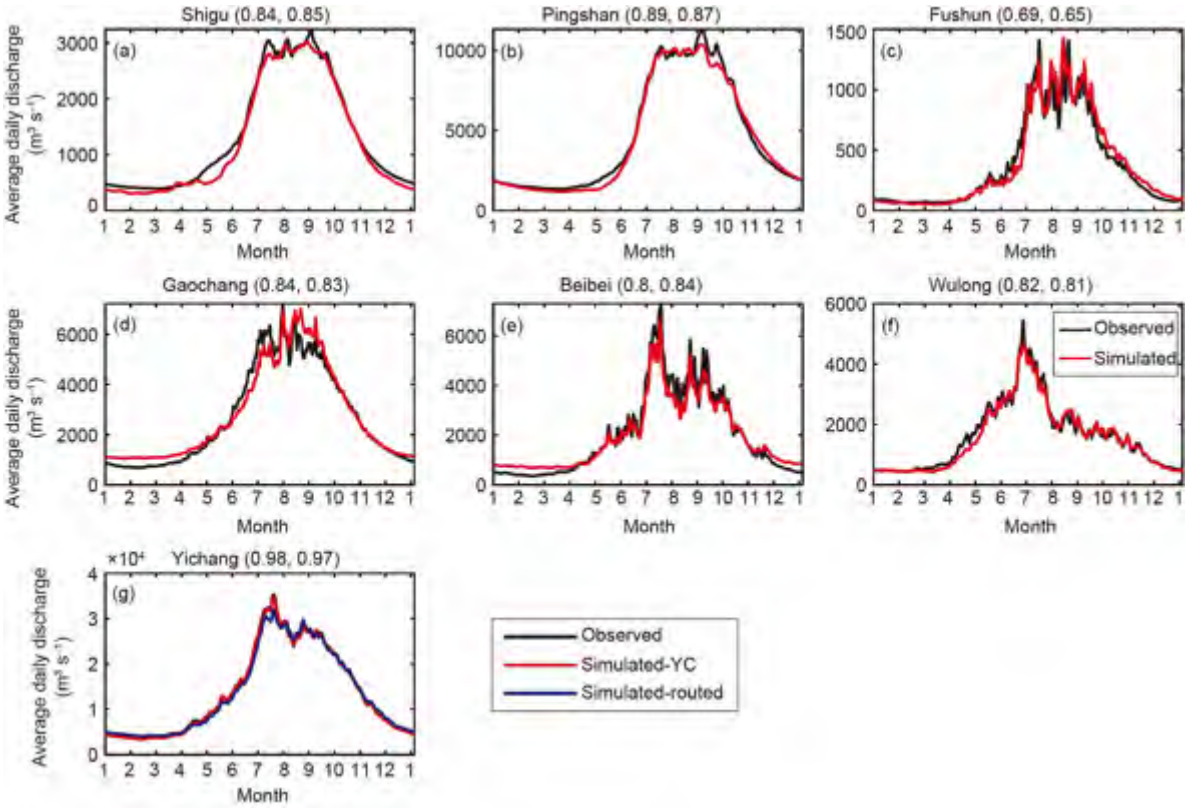

Figure 2 The calibration and validation results of the XAJ model at each subbasin during 1961–2005. The numbers in parentheses indicate the Nash-Sutcliffe coefficient of daily discharge for calibration and validation, respectively. In the plot of the Yichang subbasin, the red line represents the simulated discharge at the Yichang station (Simulated-YC), and the blue line represents the sum of the routed discharge from model simulations at upstream stations (Simulated-routed).

for the entire upper reach of the Yangtze River. 1961–1985 was selected for the calibration period and 1986–2005 was selected for the validation. The cumulative distributions of different areal indices and the statistic D of the KS test for the validation period are illustrated in Figure 3 (not shown for the calibration period). Figure 3 reveals that the distributions of bias-corrected precipitation and temperature are much closer to the observed data compared with the data from the original GCMs, although variabilities exist among different GCMs. This can also be demonstrated by the statistic D of the KS test. The critical value of the two-sample KS test for a significance level of 0.05 (the size of both samples is 20 in the validation period) from the critical value table is 0.43. This result showed that the DBC bias-corrected variables passed the KS consistency check at the 0.05 significance level. In other words, bias-correction methods could effectively reduce the D values. In addition, the correction performance of temperature is better than that of precipitation, and annual precipitation is better corrected than the maximum 1-day precipitation, as expected.

4.1.3 Evaluation of simulated daily discharge

Comparisons of the simulated discharge using observed precipitation and temperature as inputs (OBS-simulated) with that using bias-corrected or original GCM precipitation and temperature (DBC-GCM-simulated or ORI-GCM-simulated) for subbasin outlets are presented in Figures 4 and 5 for average annual hydrographs and cumulative distributions of annual maximum discharge, respectively. In Figure 4, the green uncertainty band and purple band represent daily discharges simulated using the four DBC-GCM-simulated or ORI-GCM-simulated data. It shows that (1) the hydrographs of DBC-GCM-simulated data are more consistent with those of OBS-simulated data, (2) the ORI-GCM-simulated data are highly overestimated compared with OBS-simulated data, owing to the overestimation of annual precipitation by ORI-GCMs (in Figure 3), and (3) large uncertainties of the simulations based on original GCM data are narrowed considerably after bias-correction for the entire study area, which indicates the high applicability of the DBC method for hydrological simulations. Figure 5 shows that in all basins, the cumulative distributions of DBC-GCM-simulated extremes are closer to those of OBS-simulated extremes compared with the ORI-GCM-simulated data. This demonstrates that we obtain an improved modeling performance on discharge extremes after applying DBC. Deviations among the different GCM models are also reduced after bias-correction. Even though bias still exists after bias-correction, as

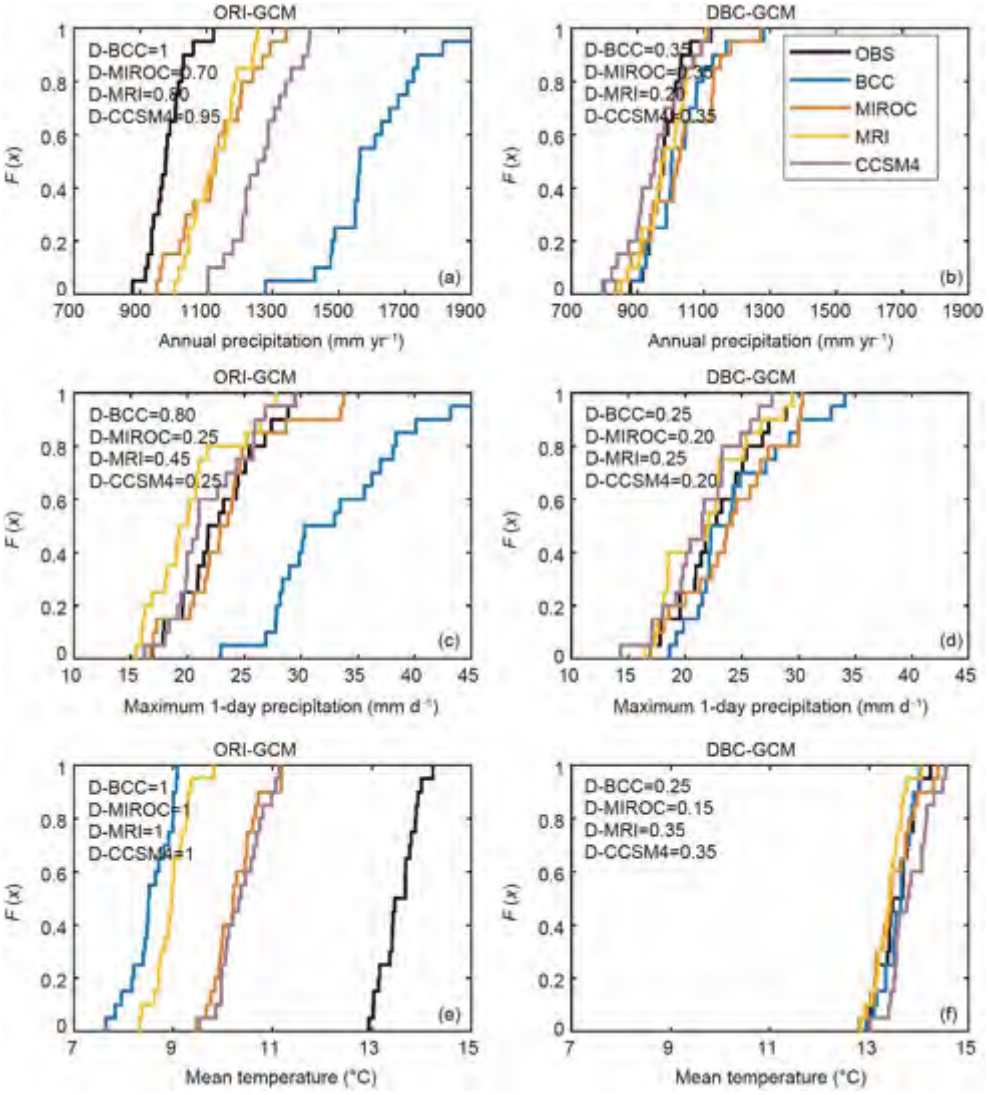

Figure 3 The cumulative distribution of original and bias-corrected indices (annual precipitation, maximum 1-day precipitation, and annual mean temperature) from four GCM models compared with observations in the upper reach of the Yangtze River during the validation period. The numbers in the legend are the statistic D of the Kolmogorov-Smirnov test. The critical value of the two-sample KS test at a significance level of 0.05 (with the size of two samples as 20 in the validation period) is 0.43, indicating that DBC bias-corrected variables pass the KS test at the 0.05 significance level.

seen at the Beibei, Wulong and Yichang stations, in general, the DBC method is able to correct the large discrepancies in precipitation and temperature for the observed vs. the original GCM series. In addition, the results reveal remarkable variances among different GCMs in some basins, such as Beibei.

4.2 Precipitation and temperature anomalies during 850–2099

Figure 6 shows the area-averaged time series of annual mean temperature anomalies over the seven subbasins of the upper reach of the Yangtze River during the period from 850 to 2099. Figures 7 and 8 show a similar presentation of the annual precipitation and maximum 1-day precipitation anomalies. The black dashed lines marking 2006 on the X-axis in the subfigures represent separating the historical period (1850–2005) and the future period (2006–2099). Please note that the data of Figures 6, 7, and 8 are smoothed by 30-yr moving averaging, and all the projected precipitation and temperature anomalies in the GCM models are bias-corrected based on historical observations. The double *y*-axis was used to distinguish the variability of precipitation and temperature over the past 1,000 years (left *y*-axis) from a significant trend for the future (right *y*-axis). The baseline period used for calculating anomalies in Figures 6–8 is 1971–2000. Based on the division of the MCA (warm period: 900–1200) and LIA (cold period: 1400–1849) periods for the past 1,000 years in Section 3.4, several hydrological indices from different GCMs during the MCA and LIA are

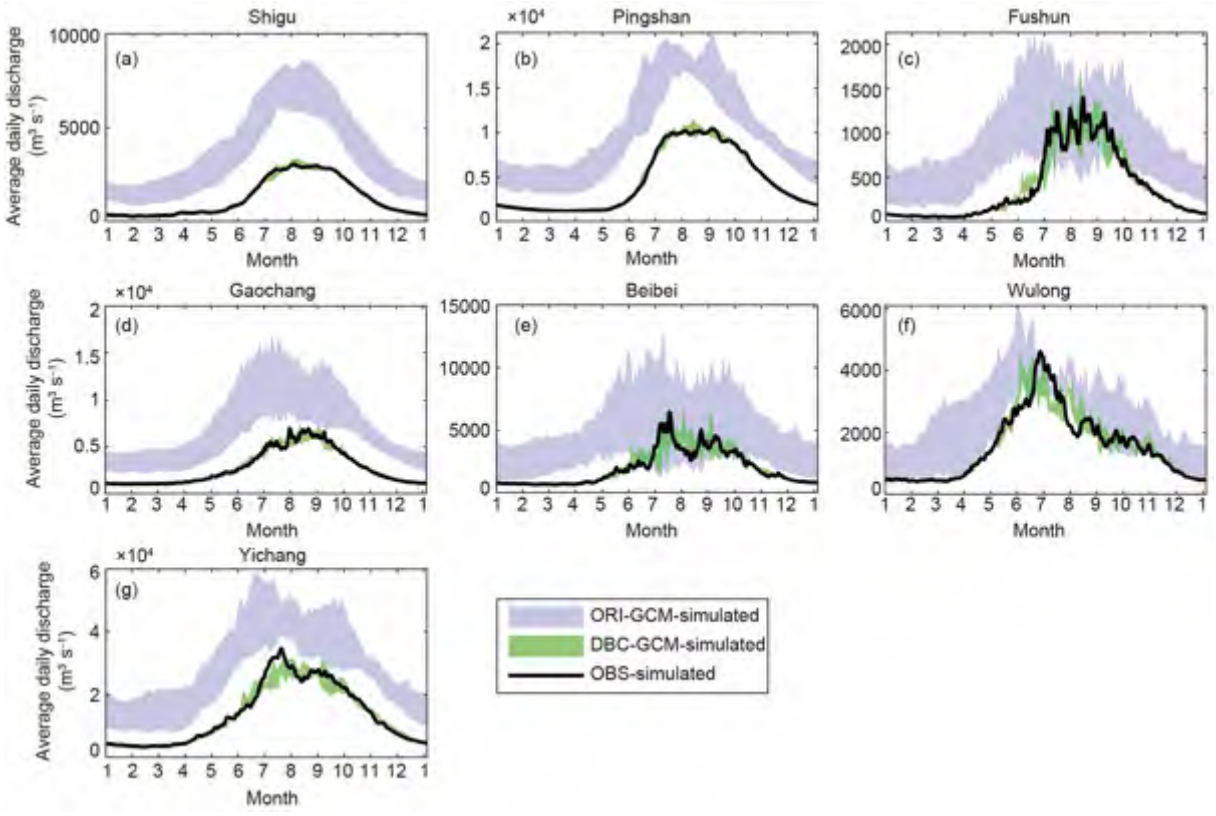

Figure 4 Average annual hydrographs for the reference period (1961–2005) in the seven subbasins. The black lines represent XAJ-simulated discharge from observed precipitation and temperature. The green uncertainty band and purple uncertainty band are the simulated daily discharges from DBC bias-corrected data and original data of four GCM models, respectively.

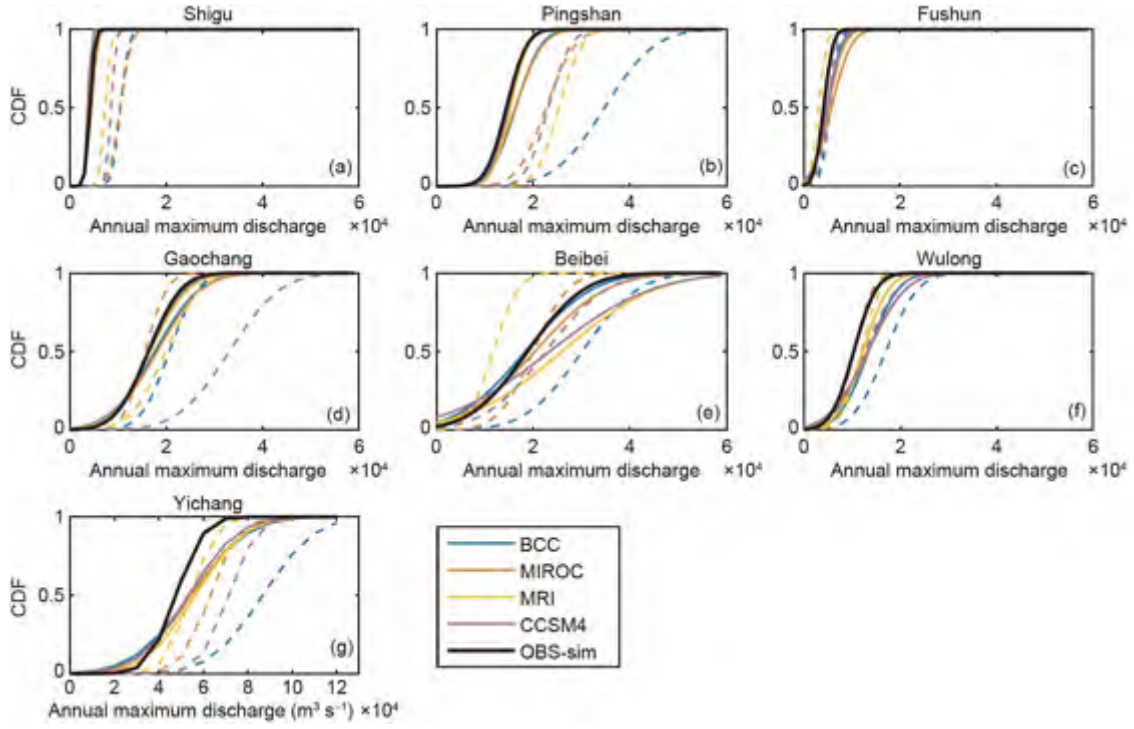

Figure 5 Cumulative distribution functions (CDFs) of the annual maximum discharge of XAJ simulated from the four GCMs and observed meteorological data during the 1961–2005 period for the seven subbasins. The dotted lines and solid lines represent the results from the original GCMs and corrected GCMs, respectively.

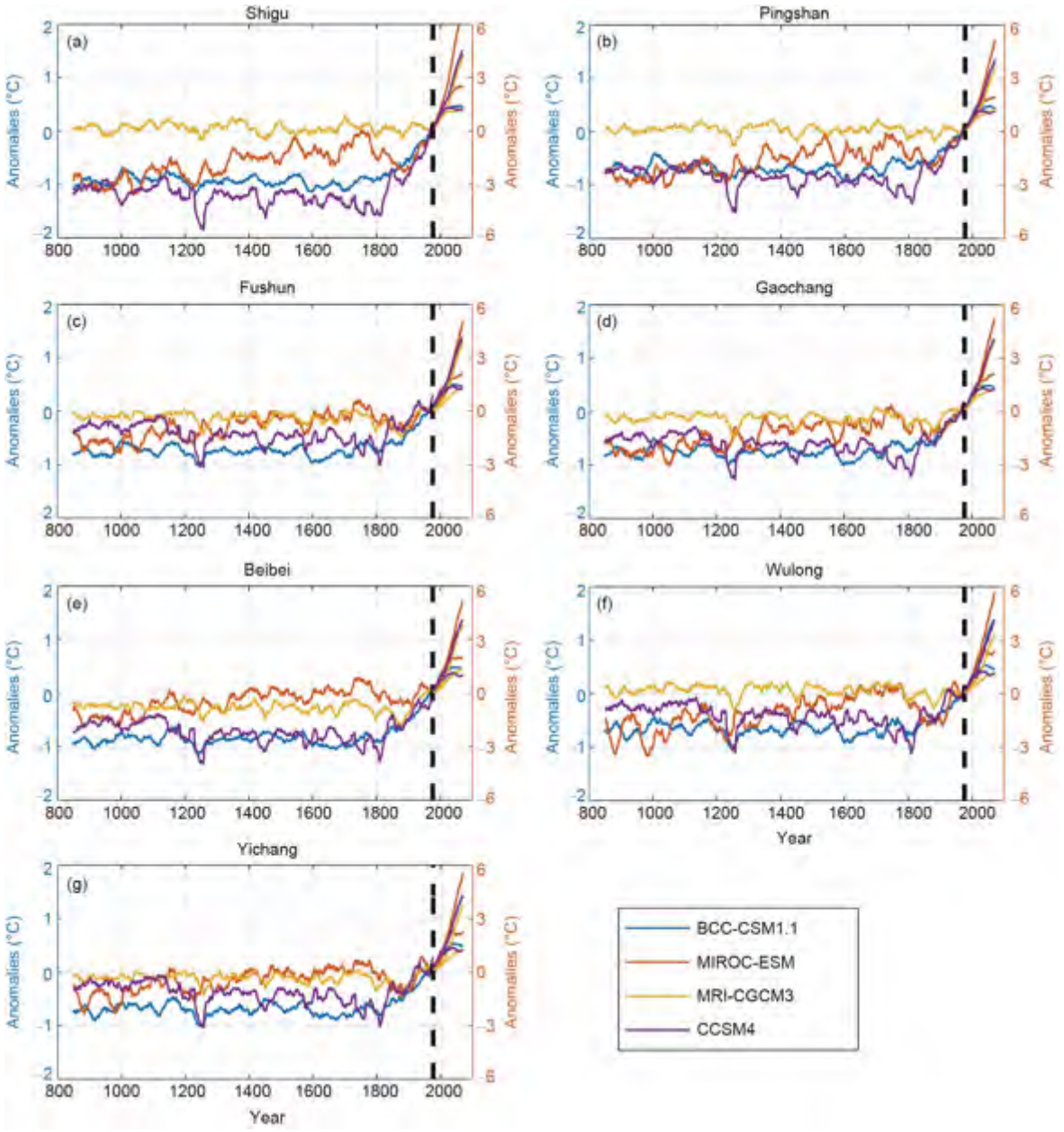

Figure 6 Annual mean temperature anomalies in each subbasin relative to 1971–2000 from four GCM models during 850–2099. The double *y*-axis was used to distinguish the variability over the past 1000 years (left *y*-axis) from a significant trend for the future (right *y*-axis). The lower and upper bounds of the uncertainty bands represent the future values of the RCP2.6 and RCP8.5 scenarios, respectively.

calculated and compared. For example, for the basin-averaged mean annual temperature, we found that it decreased by 0.03–0.31°C from the MCA to the LIA period in the subbasins of the upper Yangtze River for the BCC-CSM1.1, MRI-CGCM3, and CCSM4 models. Specifically, the temperature change of the CCSM4 model from warm to cold periods was most pronounced. However, compared to other models, the MIROC-ESM model presented a warmer temperature for different subbasins during LIA, with an increase of 0.35–0.51°C. Similarly, those hydrological indices between the LIA and the historical period (1850–2005) were also calculated for all basins. We found that for the BCC-CSM1.1 and CCSM4 models, the basin-averaged mean annual temperature increased in the range of 0.39–0.78°C from the LIA to the historical period. The MIROC-ESM and MRI-CGCM3 models, however, showed smaller changes compared with the others, ranging from −0.12 to +0.06°C. For the future trend, a pattern of positive anomalies is indicated for both the RCP2.6 and RCP8.5 future temperature projections from the four GCM models for all subbasins. In conclusion, the BCC-CSM1.1 and CCSM4 models showed better performance of a long-term temperature trend in the upper Yangtze River Basin.

The annual precipitation anomalies for the four GCMs in

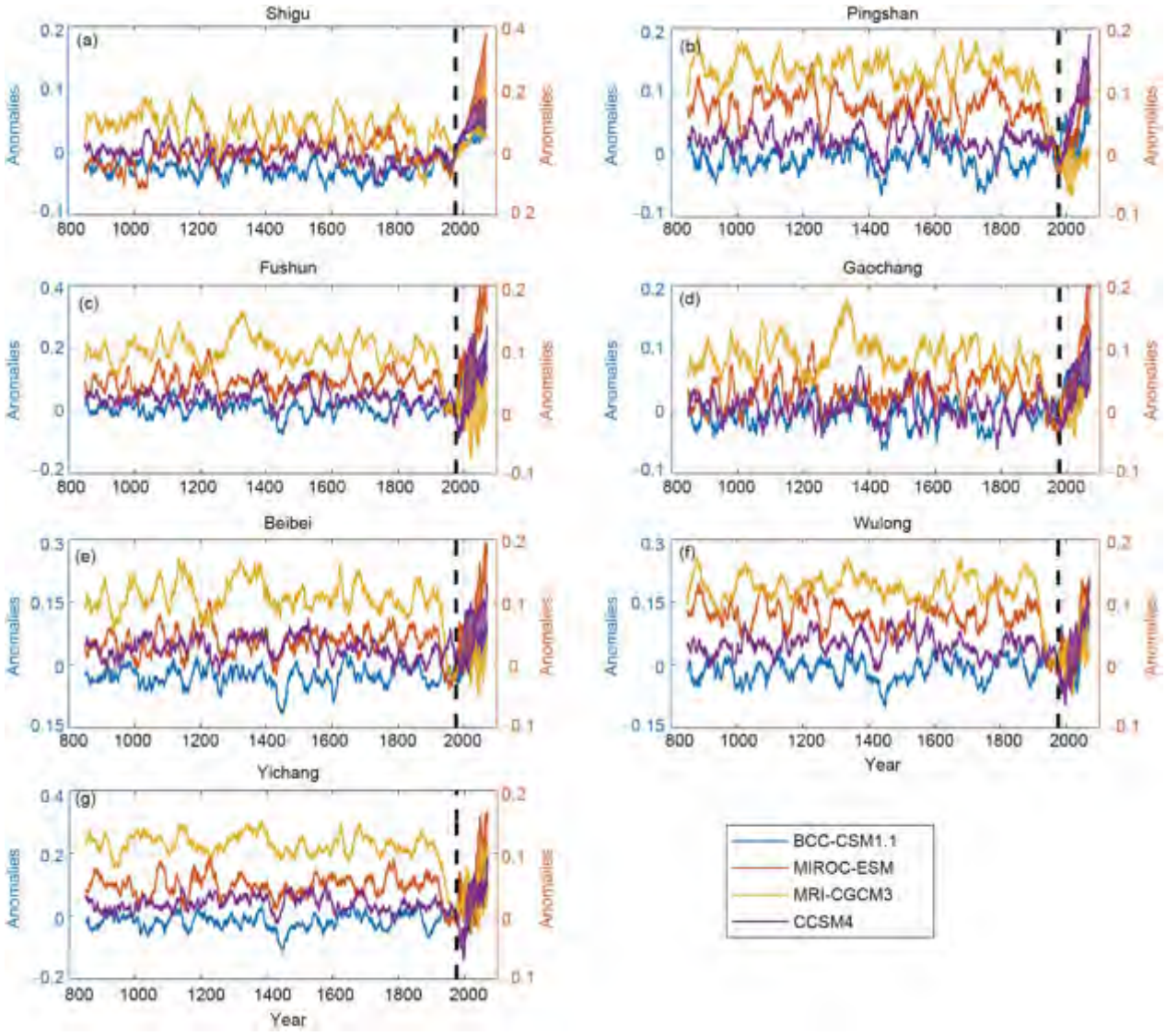

Figure 7 Annual precipitation anomalies in each subbasin relative to 1971–2000 from four GCM models from 850 to 2099. The double *y*-axis was used to distinguish the variability over the past 1,000 years (left *y*-axis) from a significant trend for the future (right *y*-axis). The lower and upper bounds of the uncertainty bands represent the future values of the RCP2.6 and RCP8.5 scenarios, respectively.

each subbasin are presented in Figure 7. An obvious decrease in annual precipitation can be seen at approximately 1400 for the BCC-CSM1.1 and CCSM4 models in almost all subbasins, which is in a period of transition from warm to cold. We compared the mean annual precipitation between MCA and LIA. From the warm to the cold period, the precipitation change of different subbasins varies from −0.89% to +0.48% for BCC-CSM1.1 (only the Pinshan basin for positive change), −1.17% to +2.53% for MIROC-ESM, −0.91% to +0.28% for MRI-CGCM3 and −1.79% to +0.90% for the CCSM4 model. Besides, the change in mean annual precipitation from LIA to the historical period presented an interval in all subbasins from −0.0007% to +1.64% for BCC-CSM1.1 (only the Pinshan basin had a negative value), from −3.42% to −1.81% for MIROC-ESM, from −6.04% to −3.08% for MRI-CGCM3 and from −2.34% to +0.63% for the CCSM4 model. Overall, the BCC-CSM1.1 model shows decreasing annual precipitation from the warm to the cold period and higher values in the historical period relative to the LIA period, which seems to be consistent with the climate change from the last millennium (warm and cold periods) to the historical period (approximately the mid-19th–late 20th century). The annual precipitation of all models will likely increase after 2005 until the end of the twenty-first century under both RCP scenarios.

The maximum 1-day precipitation (Figure 8) presents more drastic variability than the annual precipitation. Furthermore, the changes in the basin-averaged mean maximum 1-day precipitation from MCA to LIA range between −1.86% and +1.59% for BCC-CSM1.1, −0.53% and +3.84%

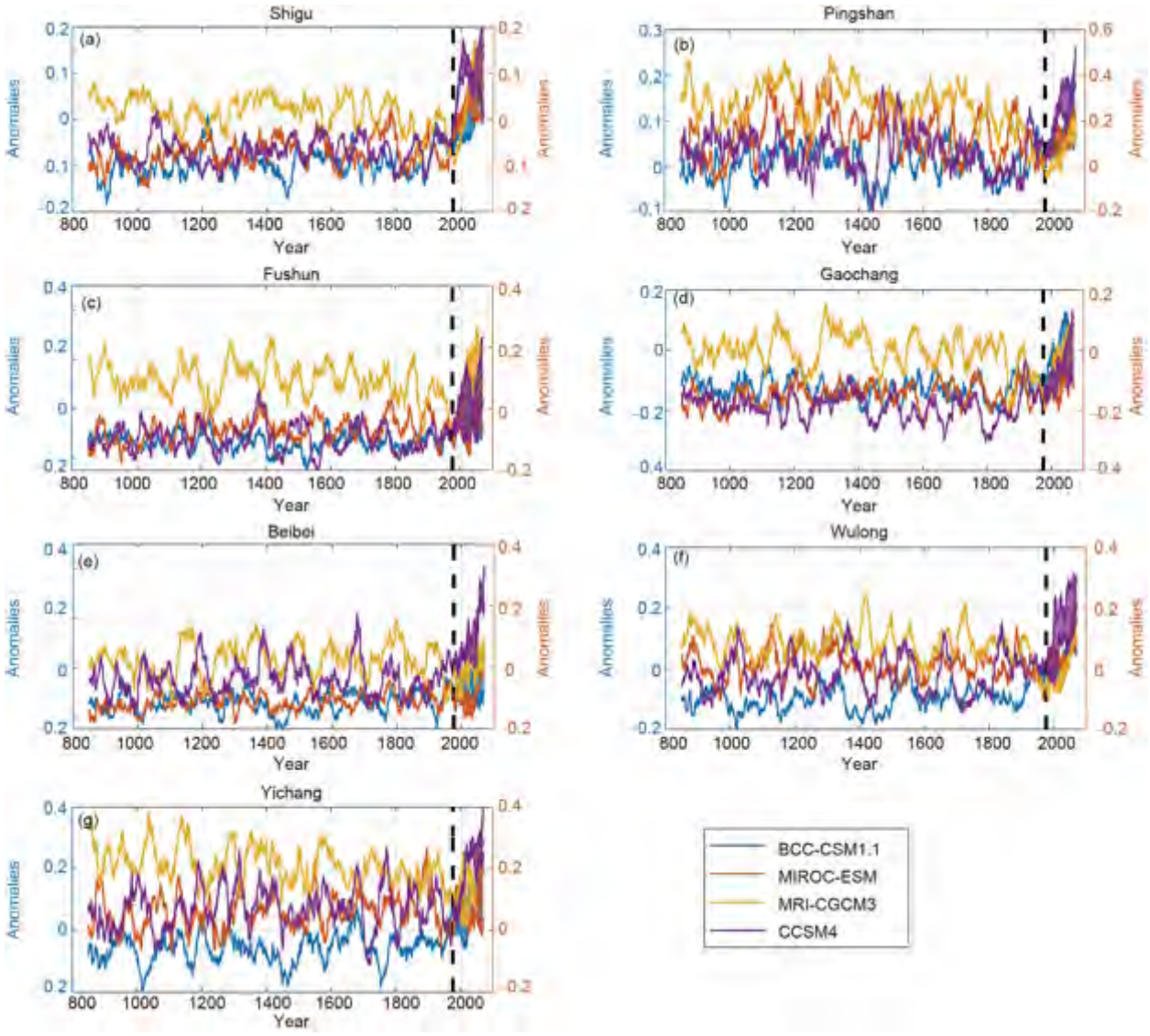

Figure 8 The maximum 1-day precipitation anomalies in each subbasin relative to 1971–2000 from four GCM models during 850–2099. The double *y*-axis was used to distinguish the variability over the past 1,000 years (left *y*-axis) from a significant trend for the future (right *y*-axis). The lower and upper bounds of the uncertainty bands represent the future values of the RCP2.6 and RCP8.5 scenarios, respectively.

for MIROC-ESM, −2.93% and +1.41% for MRI-CGCM3, and −2.32% and +3.38% for CCSM4. We found that the mean of extreme precipitation may increase or decrease in the cold period relative to the warm period for different subbasins, even for the results of the BCC-CSM1.1 model, with a better performance in general. This is probably because extreme precipitation is a regional rather than global event, which may occur in warm or cold periods due to sudden climate change. Moreover, for the changes in basin-averaged mean maximum 1-day precipitation from LIA to the historical period, the BCC-CSM1.1 model presented a positive change (+0.28% to +3.93%) in extreme precipitation for the historical period in all subbasins. However, the projected positive or negative changes could be observed in different subbasins for other models (−2.11% to +2.38% for MIROC-ESM, −8.01% to −4.63% for MRI-CGCM3 and −1.60% to +4.79% for CCSM4). In addition, the maximum 1-day precipitation of all stations is projected to increase in future climate change scenarios.

There are differences in precipitation and temperature data from different GCMs in each simulation (last millennium/historical/rcp26/rcp85). Factors that may be responsible for the great intermodal spread in precipitation and temperature change include differing climate forcings and climate feedbacks (Atwood et al., 2016). In addition, it should be noted that, unlike temperature anomalies, the variability of precipitation anomalies tends to be complex from a temporal perspective.

4.3 Paleoflood evaluation for the past 1000 period

According to the chronology of drought-flood over

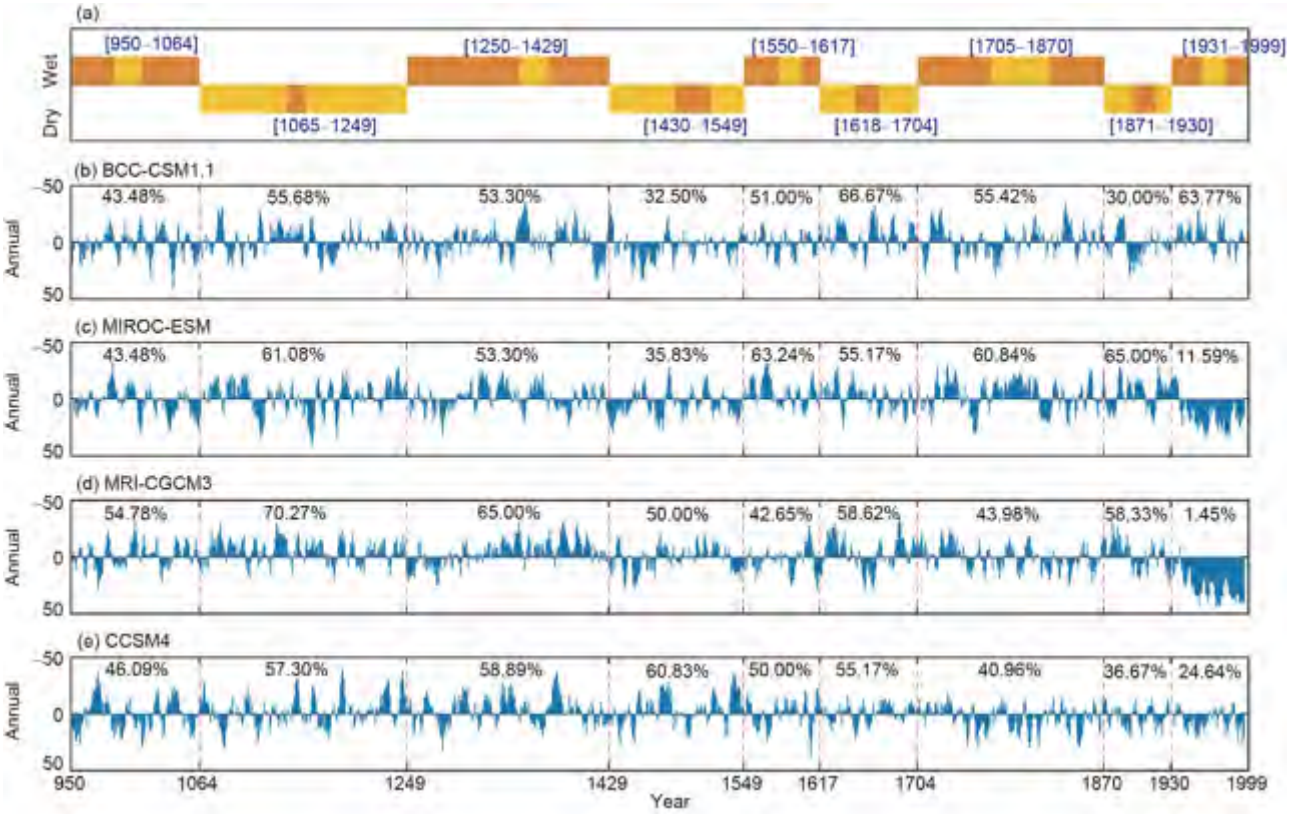

Figure 9 The anomalies of the 5-year moving averaged frequency of annual precipitation. In the upper panel graph, the upper bars indicate wet periods and the lower mean dry periods. Heavy orange represents the flood period, and light orange represents the drought period. The values in each subplot represent the percentage of negative anomaly values for each period.

1,000 years and the atlas of drought-flood distribution over 500 years in China, changes in the major dry-wet climate and minor drought-flood period in the Yangtze River during the last millennium were organized and are shown in Table 3. Based on the statistics of flood years, average years, and drought years in the study of Huang (2003), we calculated the ratio of drought and flood years in each period (see the last column of Table 3). There are 37 stations evenly distributed to the east part of 100°E in the Yangtze River basin based on the drought-flood data, so we only calculated the precipitation indices, including annual precipitation and precipitation in the flood season, for the east part of 100°E in the Yangtze River basin. The anomalies of the 5-year moving average frequency for annual precipitation and precipitation in the flood season over the last millennium are shown in Figures 9 and 10 based on the methodology of Section 3.3.2. We compared the modeled wet/dry period with the documented wet/dry period (Table 4). If the simulated and documented wet/dry periods overlap, then we believe that the simulations agree with the documented wet-dry period. In Figure 9, the proportions of frequency anomalies less than 0 for the BCC-CSM1.1 model are 53.30%, 51.00%, 55.42%, and 63.77% during the periods of 1250–1429, 1550–1617, 1705–1870, and 1931–1999, respectively, indicating consistency with documented wetness in these four periods. Similarly, the simulated lower annual precipitation in 1430–1549 and 1871–1930 from the BCC-CSM1.1 model has a good corresponding relation with documented major dryness in these two periods. Compared with BCC-CSM1.1, the simulated climate from the other models is less in agreement with the recorded dry-wet periods. Specifically, there is only some consistency in the periods of 1250–1429, 1430–1549, 1550–1617, and 1705–1870 for MIROC-ESM, 950–1064 and 1250–1429 for MRI-CGCM3, and 1250–1429, 1550–1617, and 1871–1930 for CCSM4. Meanwhile, a similar performance of these four models is also shown in Figure 10 for the indicator of precipitation in the flood season. However, there are also some discrepancies in the same GCM model between the two precipitation indices (precipitation in the flood season and annual precipitation), indicating dry or wet conditions. Considering the BCC-CSM1.1 model as an example, in the wet period 1250–1429, the proportion of negative frequency anomalies is 53.30% for annual precipitation and 43.89% for precipitation in the flood season. Overall, the BCC-CSM1.1 model has the best performance in simulating the dry-wet period of the upper Yangtze River Basin compared with other models in our study. In addition, it is not easy to capture the characteristics of minor drought-

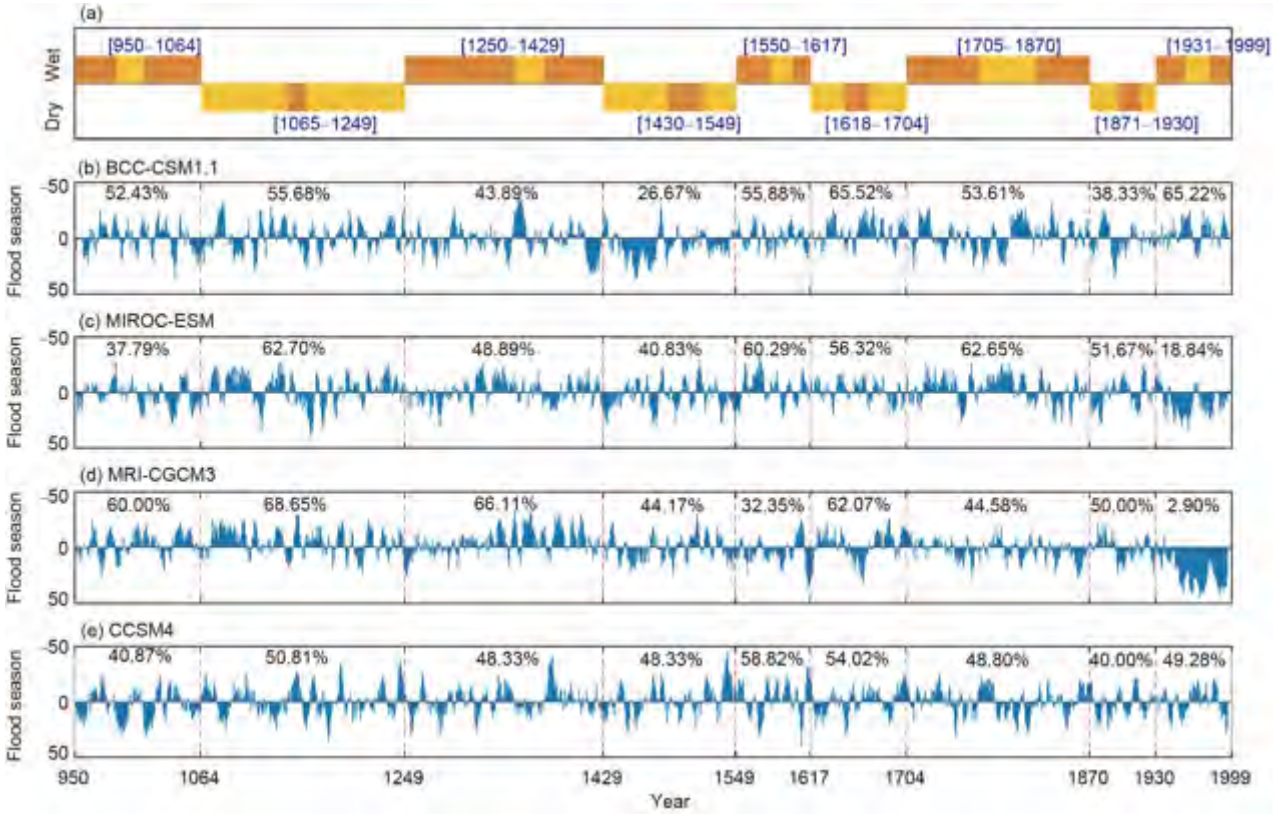

Figure 10 The anomalies of the 5-year moving averaged frequency of flood season precipitation. In the upper panel graph, the upper bars indicate wet periods and the lower mean dry periods. Heavy orange represents the flood period, and light orange represents the drought period. The values in each subplot represent the percentage of negative anomaly values for each period.

flood periods compared with those of major dry-wet periods for almost all GCMs.

The magnitude and time of each paleoflood event listed in Table 1 are presented in Figure 11 using black circles and dashed lines, respectively. Furthermore, the 10-year moving average of the maximum 1-day discharge at Yichang station during the period of 900–2000 for four DBC-GCM-simulated discharges is presented in Figure 11. In general, there are some common features in GCM-simulated extreme discharge and reconstructed paleofloods. Specifically, the important paleofloods occurred primarily during the periods of 1100–1300, 1600–1800, and 1850–2000 (gray bars in Figure 11), when the frequency of relatively larger floods in the mainstream of the upper reach of the Yangtze River was also higher in the same three periods. We calculated the frequency of maximum 1-day discharge higher than the average value per 100 years for each model and counted the average frequencies of some specific periods in Table 5. The average frequencies during the periods of 1100–1300, 1600–1800, and 1850–2000 are 47%, 42%, and 44%, respectively, which are all greater than the frequency (39%) in 1300–1600 for the BCC-CSM1.1 model. However, the frequency of other models shows some inconsistency compared with the record. Since this reconstruction-model comparison focuses on the common relative changes rather than on the magnitude and the absolute values, the results of BCC-CSM1.1 indicate the relative consistency between the model-simulated extreme discharge and the reconstructed paleofloods.

Figure 11e shows the change in reconstructed temperature in Eastern Qinghai-Xizang Plateau and Central-East China during 900–2000 (Ge et al., 2017). There was a warm period from 900 to 1200 for the Eastern Qinghai-Xizang Plateau and Central-East China; however, the time when the temperature decreased differed for these two regions. Temperature shows a fluctuating downward trend from 1200 to 1850 for Eastern Qinghai-Xizang Plateau and from 1300 to 1850 for Central-East China. Finally, the Little Ice Age ends in 1850, and the temperature has risen significantly since then. The temperature anomalies from BCC-CSM1.1, MRI-CGCM3, and CCSM4 (see Figure 6) present a decreasing trend since 1200 for all subbasins.

In addition, we can see that reconstructed paleofloods and DBC-GCM-simulated extreme discharge occurred in the warm period or cold period for the mainstream of the upper reach of the Yangtze River. Part of the explanation is that more water vapor is transported by the southwest monsoon during the warm period, resulting in more precipitation in the upper reach of the Yangtze River. However, although the

Table 3 The changes in the major dry-wet climate and minor drought-flood period in the Yangtze River Basin during the last millennium[a)]

Major dry-wet climate		Minor drought-flood period		
Dry or wet period	Time range	Drought-flood period	Time range	Drought-flood ratio
Wet period	950–1064	Flood	950–988	0.17
		Drought	989–1012	5.50
		Flood	1013–1064	0.36
Dry period	1065–1249	Drought	1065–1142	2.00
		Flood	1143–1159	0.44
		Drought	1160–1249	1.89
Wet period	1250–1429	Flood	1250–1349	0.56
		Drought	1350–1375	2.00
		Flood	1376–1429	0.20
Dry period	1430–1549	Drought	1430–1489	1.75
		Flood	1490–1519	0.40
		Drought	1520–1549	5.00
Wet period	1550–1617	Flood	1550–1580	0.29
		Drought	1581–1600	3.00
		Flood	1601–1617	0.11
Dry period	1618–1704	Drought	1618–1648	1.40
		Flood	1649–1670	0.44
		Drought	1671–1704	1.30
Wet period	1705–1870	Flood	1705–1769	0.47
		Drought	1770–1821	1.67
		Flood	1822–1870	0.63
Dry period	1871–1930	Drought	1871–1895	1.80
		Flood	1896–1917	0.78
		Drought	1918–1930	7.00
Wet period	1931–1999	Flood	1931–1957	0.63
		Drought	1958–1979	4.00
		Flood	1980–1999	0.27

a) The drought-flood ratio equals the number of drought years divided by the number of flood years

Table 4 Comparisons between documented wet/dry periods and modeled wet/dry periods[a)]

Time range	Record	BCC-CSM1.1	MIROC-ESM	MRI-CGCM3	CCSM4
950–1064	Wet	Dry/Wet	Dry/Dry	Wet/Wet	Dry/Dry
1065–1249	Dry	Wet/Wet	Wet/Wet	Wet/Wet	Wet/Wet
1250–1429	Wet	Wet/Dry	Wet/Dry	Wet/Wet	Wet/Dry
1430–1549	Dry	Dry/Dry	Dry/Dry	Wet/Dry	Wet/Dry
1550–1617	Wet	Wet/Wet	Wet/Wet	Dry/Dry	Wet/Wet
1618–1704	Dry	Wet/Wet	Wet/Wet	Wet/Wet	Wet/Wet
1705–1870	Wet	Wet/Wet	Wet/Wet	Dry/Dry	Dry/Dry
1871–1930	Dry	Dry /Dry	Wet/Wet	Wet/Wet	Dry/Dry
1931–1999	Wet	Wet/ Wet	Dry/Dry	Dry/Dry	Dry/Dry

a) The modeled wet/dry periods indicate annual precipitation and precipitation in the flood season

climate became cooler and drier as well as precipitation decreased during the transition from MCA to LIA, floods may have occurred due to an uneven spatial-temporal distribution of precipitation.

Table 5 The frequency of maximum 1-day discharge larger than the average value for different time periods for each model

Statistical periods	BCC-CSM1.1	MIROC-ESM	MRI-CGCM3	CCSM4
1100–1300	47%	67%	84%	43%
1300–1600	39%	61%	83%	47%
1600–1800	42%	62%	80%	47%
1850–2000	44%	57%	70%	49%

4.4 Changes in extreme discharge from the last millennium to the end of the 21st century

To explore changes in DBC-GCM-simulated extreme discharge from the last millennium to the future, large floods with upper-quantiles (0.75, 0.90, and 0.95) and small floods with lower-quantiles (0.05, 0.10, and 0.15) of maximum 1-day discharge were calculated in each subbasin for each GCM of various experiments in the MCA, LIA, RCP2.6, and RCP8.5 periods (Figures 12 and 13). Considering the best performance of the BCC-CSM1.1 model in comparison with recorded dry-wet periods and observed temperature anomalies for the last millennium, we focus on the result of this model. Figure 12 shows that (1) climate change led to a 0.78–10.38% decrease in the magnitude of large floods for the different quantiles (0.75, 0.90, and 0.95) during the LIA relative to the period 900–1200 for all subbasins except the Pingshan basin, and (2) large floods for subbasins during the historical period (1912–2005) increased 0.23–12.86% over the LIA period for most subbasins. The lower-quantile extreme values (small floods) generally showed a similar change from the last millennium to the historical period compared with that of upper-quantile values, with exceptions in some basins. Further comparison between historical and RCP2.6&8.5 values demonstrates a significant increase in extreme discharges under the enhanced greenhouse gas warming, and the trend is higher in high emission scenarios for almost all subbasins.

5. Discussion

5.1 Uncertainty leading to differences between modeled extreme discharge and reconstructed paleoflood events

In this study, we explored comparisons between paleoflood data and model simulations and found some agreement between the DBC-GCM-simulated extreme discharge and reconstructed paleofloods during the last millennium. The simulated extreme discharge from GCMs using the hydrological model and reconstructed floods from the water level are found to be broadly consistent with the patterns of atmospheric variability in the upper reach of the Yangtze River, for example: the drying phenomenon from the mid-11th to the mid-13th century and in the late 1800s and early 1900s, as well as wetting during the 1250–1429 and 1550–1617 periods. However, there are also differences between DBC-GCM-simulated extremes and reconstructed flood records, which may be attributed to inaccuracy in data for precipitation and temperature from the GCMs. The coarse spatial resolution of the GCMs gives imperfect representations of the physical processes and topographic features which, however, are important for understanding regional hydroclimate. Another possibility is that the grids of the GCMs are unrepresentative of the drought-flood estimate provided by 37 stations (point). Prior studies comparing models and proxy data have found several disagreements between them. There is more hydroclimate variability in the proxy data than in the models in the last millennium, and the droughts and wetness periods in the CMIP5 precipitation simulation are not precisely temporally synchronous with those in the proxy data (Seftigen et al., 2017). Furthermore, we can also see that the variability of maximum 1-day precipitation and discharge is not dramatic, and there are some discrepancies between reconstructed dry-wet periods and GCM precipitation (annual precipitation and precipitation in flood season) in our study. In addition, Ljungqvist et al. (2016) compared CMIP5 simulations of precipitation and reconstructed hydroclimate in the Northern Hemisphere and pointed out that, despite existing biases, models could contribute to useful understandings of the characteristics and variability of pre-instrumental hydroclimate data.

Other uncertainties stem from differences between projections among the GCMs. For example, the 20th century is characterized by major wetness and high-frequency floods from the dry-wet record and paleoflood (Figures 9–11), while the extreme precipitation and discharge of MIROC-ESM and MRI-CGCM3 show opposite performance over the 20th century. However, BCC-CSM1.1 is consistent with the recorded wetness and a flood-prone period. The literature also demonstrates that BCC (Beijing Climate Center Climate System) models (e.g., BCC-CSM1.0, BCC-CSM1.1, BCC-CSM1.1 (m)) can reproduce the basic features of the observed climatology of annual total precipitation and extreme precipitation in China (Zhang et al., 2011; Wang et al., 2016). The study reveals that the MIROC-ESM model exhibits possible drifts for the long-term trends of surface temperature (Bothe et al., 2013; Gupta et al., 2013; Lewis and LeGrande, 2015), which is consistent with our results in Figure 6, showing a fluctuating and increasing trend during the

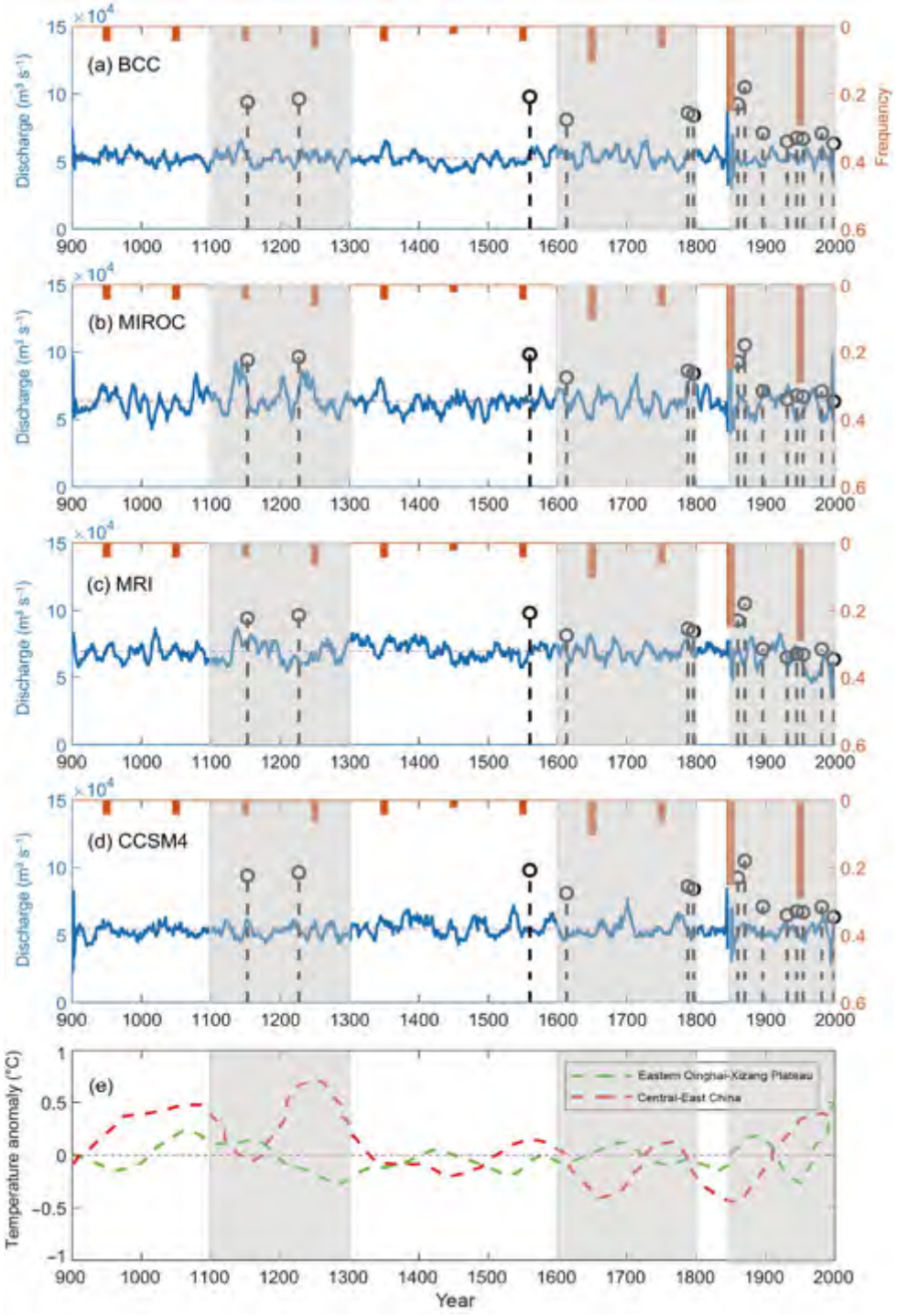

Figure 11 The 10-year moving average of the maximum 1-day discharge at Yichang station during the period of 900–2000 for the four GCM-simulated discharges (blue solid line). The pink dashed line represents the average annual maximum 1-day discharge; the black circle and dashed line represent the magnitude and time of paleoflood events from reconstruction at Yichang station; the orange bar represents the frequency of major floods and floods with inscriptions in the mainstream of the upper reach of the Yangtze River. The frequency values are obtained by dividing the number of recorded floods per 100 years by the total number during the period of 900–2000. The last row of this plot indicates the change in temperature series in Eastern Qinghai-Xizang Plateau and Central East China since 900 AD (Ge et al., 2017). The gray bars represent the periods in which floods occur frequently in the upper Yangtze River Basin.

period of 850–2005. Therefore, possible biases or errors of precipitation and temperature data in the model simulation would lead to relatively larger differences in extreme discharge results and reconstructed paleofloods.

In general, the biases of GCM outputs (precipitation and temperature) and differences among climate models will

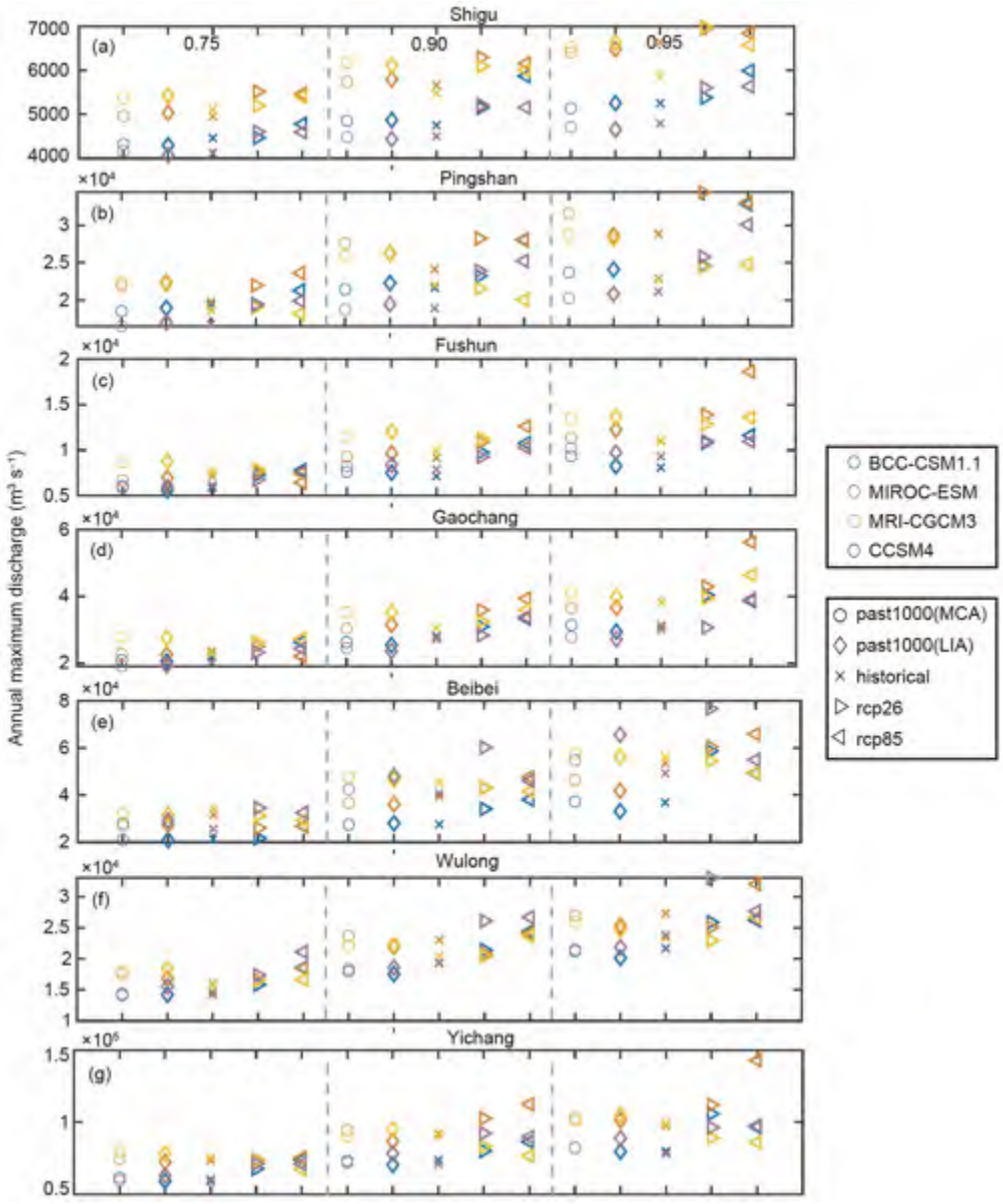

Figure 12 Comparison of large floods with upper-quantiles (0.75, 0.90, and 0.95) for maximum 1-day discharge in each subbasin for each GCM of various experiments in the MCA, LIA, history, RCP26, and RCP85 periods (shown by different markers). Each column shows the results of the four GCMs. The past 1,000 data have been bootstrap-resampled to the same length as the future time series.

inevitably lead to differences in runoff responses (floods) to climate change. Moreover, other sources (e.g., bias-correction methods and hydrological models) of uncertainty in discharge simulations should also be considered (Lawrence and Haddeland, 2011; Zhang et al., 2021). Vormoor et al. (2015) found that climate projections (i.e., the GCMs) or the bias-correction methods tend to be the largest contributor to the overall uncertainty in the projected changes in discharge compared with different hydrological parameters. We acknowledge that using only one particular bias-correction method or hydrological model may induce uncertainty in hydrological projections. Therefore, the use of multiple bias-correction methods and hydrological models is needed for more robustly simulating past and future watershed streamflow results for more precisely estimating flood impacts in future researches.

5.2 The relationship between paleoflood events and climate change

Floods are mainly driven by hydroclimate variables, i.e., precipitation and temperature. For paleoflood reconstruction, a fundamental concern is capturing accurate climate and hydrological conditions for flood generation and understanding their variations. Changes in hydrological conditions were also discovered from other paleoenvironmental records

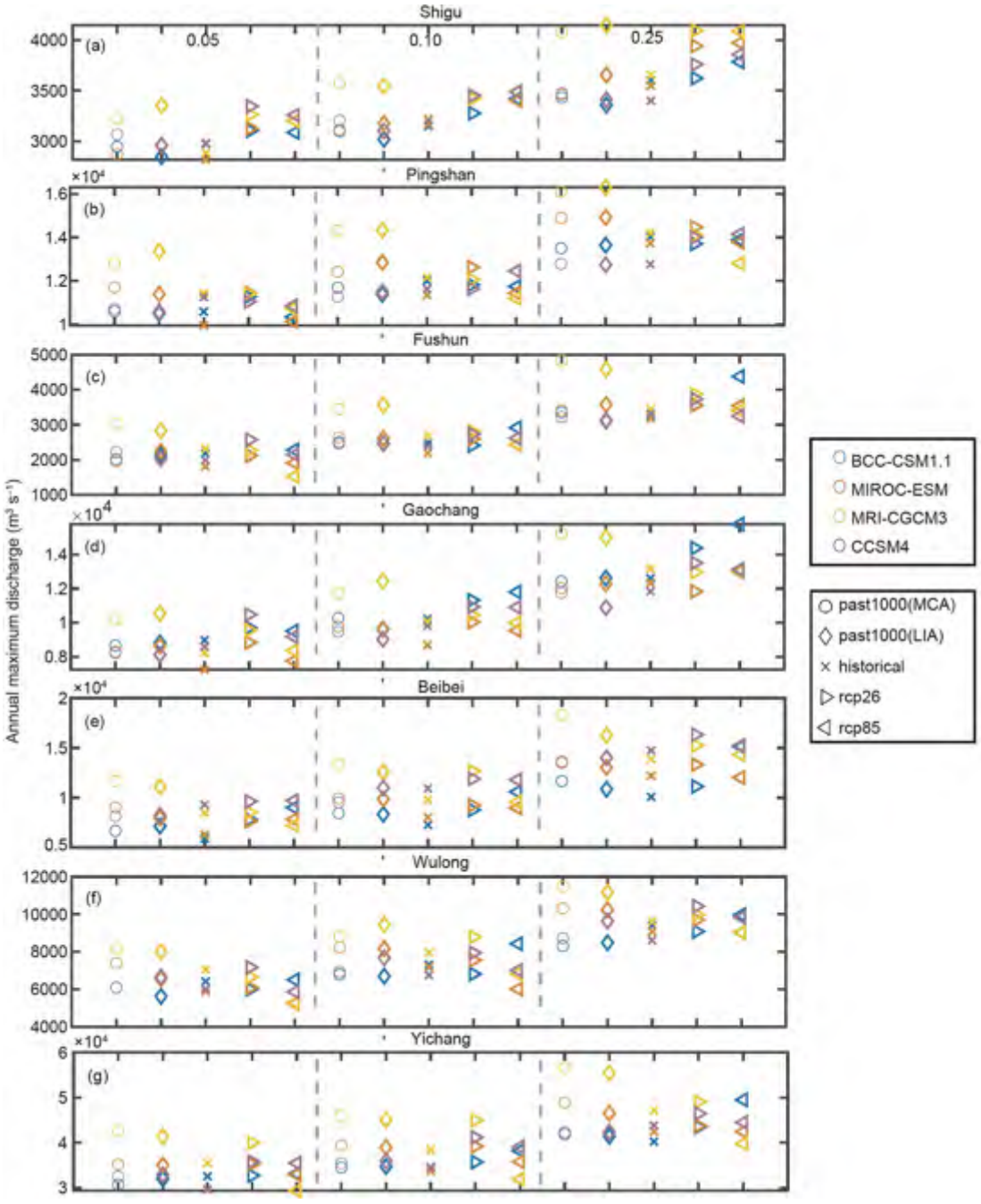

Figure 13 Comparison of small floods with lower-quantile (0.05, 0.10, and 0.15) for maximum 1-day discharge in each subbasin for each GCM of various experiments in the MCA, LIA, history, RCP26 and RCP85 periods (shown by different markers). Each column shows the results of four GCMs. The past 1,000 data have been bootstrap-resampled to the same length as the future time series.

in our study region during the last millennium. The paleofloods of 1153 and 1227 occurred in the warm period, when there was an obvious temperature rise at approximately 1200 in eastern China. In addition, there was a flood in 1560 at the beginning of the LIA period, when this period was characterized by temperature fluctuation. Tree rings from the southern Qinghai-Xizang Plateau showed a temperature decline during 1600–1800 (Wang et al., 2014), and an obvious transition was found in the dry-wet sequence in eastern China around the 17th century (Ge et al., 2007). The large flood events of 1613, 1788, and 1796 that occurred in the most volatile period of LIA were due to a sharp temperature decline. Libo stalagmite records in Guizhou (Wujiang River) show the multicycle variations of monsoon climate from weak to strong for the period of 1340–1880 (Qin et al., 2008), and the Qinghai-Xizang Plateau also appeared to experience a low-temperature point from 1600 to 1800. In addition, the 1790–1890 period was the last cold period of

the LIA in the historical records, which is the transition period at the end of the LIA, in which there were three floods, i.e., 1860, 1870, and 1896. It was recorded that the climate in China fluctuated considerably around 1850 (Chen et al., 2006). Furthermore, it is well known that major floods occurred in 1931, 1945, 1954, 1981, and 1998 since the end of the LIA in the upper reach of the Yangtze River.

In addition, we found that paleofloods occurred in both warm and cold periods. In warm and wet periods, higher annual precipitation and saturated soils could easily lead to an elevated risk of flooding in the upper Yangtze River basin, while in dry and cold periods, the basin is sensitive to extreme precipitation that can trigger rapid flash-flooding with saturated overland flow and shallow subsurface flow.

6. Conclusions

This study presents an assessment of variability and trends in climate and hydrological extremes (including precipitation, temperature, and floods) for the upper reach of the Yangtze River from the last millennium to the end of the 21st century. Both instrumental observations and historical records (i.e., wet/dry period and flood events) were integrated for model calibration and flood simulation evaluation. A number of conclusions can be drawn from this study:

(1) The performance of all GCMs, except MIROC-ESM, coincides with the documented long-term temperature variability, which reflects the difference between the MCA and LIA periods.

(2) Among all GCMs, BCC-CSM1.1 has the best performance for precipitation indices (i.e., annual and flood season precipitation) compared with the historically recorded dry-wet periods. In addition, this model's precipitation anomalies (i.e., annual and maximum 1-day precipitation anomalies) also broadly agree with the observed trend and variability changes from the last millennium (warm and cold periods) to the historical period. There are more consistencies for the frequency between reconstructed paleofloods and extreme discharge from BCC-CSM1.1 than with other models.

(3) From the BCC-CSM 1.1 model, the magnitude of extreme discharge (at different quantile values) decreases from the warm period to the cold period in most subbasins over the entire upper Yangtze River Basin. For example, the magnitude drops approximately 0.78–10.38% for upper-quantile extremes and 1.13–7.33% for lower-quantile extremes. Furthermore, we found some extreme discharge increases in the historical period compared with the LIA period. In addition, there would be a higher flood risk with larger discharge values in the future under both RCP scenarios.

Acknowledgements *The authors wish to thank the contribution of the World Climate Research Program Working Group on Coupled Modeling, which is responsible for CMIP, and would like to acknowledge climate modeling groups (listed in Table 2 of this paper) for making available their respective climate model outputs. The authors are also grateful to the Yangtze River Hydrological Bureau of China for providing the discharge data of hydrological stations in this paper. The authors also wish to acknowledge the researchers who have produced and made their paleoflood data available. This work was supported by the National Key Research and Development Program (Grant No. 2017YFA0603702) and the Research Council of Norway (FRINATEK Project 274310).*

References

Atwood A R, Wu E, Frierson D M W, Battisti D S, Sachs J P. 2016. Quantifying climate forcings and feedbacks over the last millennium in the CMIP5-PMIP3 models. J Clim, 29: 1161–1178

Bothe O, Jungclaus J H, Zanchettin D. 2013. Consistency of the multi-model CMIP5/PMIP3-past1000 ensemble. Clim Past, 9: 2471–2487

Chen J, Brissette F P, Chaumont D, Braun M. 2013. Performance and uncertainty evaluation of empirical downscaling methods in quantifying the climate change impacts on hydrology over two North American river basins. J Hydrol, 479: 200–214

Chen J, Wu X D, Finlayson B L, Webber M, Wei T Y, Li M T, Chen Z Y. 2014. Variability and trend in the hydrology of the Yangtze River, China: Annual precipitation and runoff. J Hydrol, 513: 403–412

Chen J Q, Shi Y F, Zhang Q, Zhang Z X. 2006. Climatic background for historical flood of 1860, 1870 during past 500 years in the upper Yangtze River basin (in Chinese). Sci Limnol Sin, 18: 476–483

Dong J P, Li Z J, Dai J N. 2012. Application of SCE-UA algorithm to optimization of Xin'anjiang model parameters (in Chinese). J Hohai Univ-Nat Sci, 40: 485–490

Engeland K, Aano A, Steffensen I, Støren E, Paasche Ø. 2020. New flood frequency estimates for the largest river in Norway based on the combination of short and long time series. Hydrol Earth Syst Sci, 24: 5595–5619

Gao B, Yang D, Zhao T, Yang H. 2012. Changes in the eco-flow metrics of the Upper Yangtze River from 1961 to 2008. J Hydrol, 448-449: 30–38

Ge Q, Hao Z, Zheng J, Shao X. 2013. Temperature changes over the past 2000 yr in China and comparison with the Northern Hemisphere. Clim Past, 9: 1153–1160

Ge Q, Liu H, Ma X, Zheng J, Hao Z. 2017. Characteristics of temperature change in China over the last 2000 years and spatial patterns of dryness/wetness during cold and warm periods. Adv Atmos Sci, 34: 941–951

Ge Q, Wang S, Wen X, Shen C, Hao Z. 2007. Temperature and precipitation changes in China during the holocene. Adv Atmos Sci, 24: 1024–1036

Ge Q S, Zheng J Y, Hao Z X, Shao X M, Wang W C, Luterbacher J. 2010. Temperature variation through 2000 years in China: An uncertainty analysis of reconstruction and regional difference. Geophys Res Lett, 37: L03703

Ge Z S. 2009. The response of Holocene extreme floods in the Upper Changjiang River to changes of southwest monsoon (in Chinese). Geogr Res, 28: 592–600

Hinkley D V. 1988. Bootstrap methods. J Royal Stat Soc Ser B-Methodol, 50: 321–337

Huang W H, Sui Y, Yang X G, Dai S W, Li M S. 2013. Characteristics and adaptation of seasonal drought in southern China under the background of climate change. III. Spatiotemporal characteristics of seasonal drought in southern China based on the percentage of precipitation anomalies (in Chinese). Chin J Appl Ecol, 24: 397–406

Huang Z S. 2003. Analysis of historical flood and drought disaster in Yangtze River Basin (in Chinese). Yangtze River, 34: 1–3

Huo R, Li L, Chen H, Xu C Y, Chen J, Guo S. 2021. Extreme precipitation changes in Europe from the last millennium to the end of the 21st century. J Clim, 34: 567–588

Lawrence D, Haddeland I. 2011. Uncertainty in hydrological modelling of climate change impacts in four Norwegian catchments. Hydrol Res, 42:

457–471
Lewis S C. 2018. Assessing the stationarity of Australian precipitation extremes in forced and unforced CMIP5 simulations. J Clim, 31: 131–145
Lewis S C, LeGrande A N. 2015. Stability of ENSO and its tropical Pacific teleconnections over the Last Millennium. Clim Past, 11: 1347–1360
Li C W, Huang Y, Yan L Z. 2022. Study on characteristics of over-standard flood disaster in Changjiang River Basin under changing environment (in Chinese). Yangtze River, 53: 29–43
Li T, Li J, Zhang D D. 2020. Yellow River flooding during the past two millennia from historical documents. Prog Phys Geography-Earth Environ, 44: 661–678
Li X G. 2014. The study of Holocene Palaeoflood Hydrology in the Jinshan Gorges of the Yellow River and in Baihe reach of the upper Hanjiang River (in Chinese). Dissertation for Doctoral Degree. Xi'an: Shaanxi Normal University. 1–211
Ljungqvist F C, Krusic P J, Sundqvist H S, Zorita E, Brattström G, Frank D. 2016. Northern Hemisphere hydroclimate variability over the past twelve centuries. Nature, 532: 94–98
Munoz S E, Giosan L, Therrell M D, Remo J W F, Shen Z, Sullivan R M, Wiman C, O'Donnell M, Donnelly J P. 2018. Climatic control of Mississippi River flood hazard amplified by river engineering. Nature, 556: 95–98
Nash J E, Sutcliffe J V. 1970. River flow forecasting through conceptual models part I—A discussion of principles. J Hydrol, 10: 282–290
Qin J M, Yuan D X, Lin Y S, Zhang H L, Zhang M L, Cheng H, Wang H, Yang Y, Ran J C. 2008. High resolution stalagmite records of climate change since 800a A.D. in Libo, Guizhou (in Chinese). Carsol Sin, 27: 266–272
Scussolini P, Eilander D, Sutanudjaja E H, Ikeuchi H, Hoch J M, Ward P J, Bakker P, Otto-Bliesner B L, Guo C, Stepanek C, Zhang Q, Braconnot P, Guarino M V, Muis S, Yamazaki D, Veldkamp T I E, Aerts J C J H. 2020. Global river discharge and floods in the warmer climate of the last interglacial. Geophys Res Lett, 47: e89375
Seftigen K, Goosse H, Klein F, Chen D. 2017. Hydroclimate variability in Scandinavia over the last millennium—Insights from a climate model-proxy data comparison. Clim Past, 13: 1831–1850
Gupta A S, Jourdain N C, Brown J N, Monselesan D. 2013. Climate drift in the CMIP5 models. J Clim, 26: 8597–8615
Sheng H, Xu X, Gao J H, Kettner A J, Shi Y, Xue C, Wang Y P, Gao S. 2020. Frequency and magnitude variability of Yalu River flooding: Numerical analyses for the last 1000 years. Hydrol Earth Syst Sci, 24: 4743–4761
Smith G H S, Best J L, Ashworth P J, Lane S N, Parker N O, Lunt I A, Thomas R E, Simpson C J. 2010. Can we distinguish flood frequency and magnitude in the sedimentological record of rivers? Geology, 38: 579–582
Tang X, Feng Q. 2021. Analysis of drought and flood disasters during 0–1950 AD in the Hexi Corridor, China, based on historical documents. Front Environ Sci, 9: 781179
Taylor K E, Stouffer R J, Meehl G A. 2012. An overview of CMIP5 and the experiment design. Bull Am Meteorol Soc, 93: 485–498
Tian Y. 2015. Impacts of climate change on regional and global hydrology (in Chinese). Dissertation for Doctoral Degree. Hangzhou: Zhejiang University. 1–100
Tschöke G V, Kruk N S, de Queiroz P I B, Chou S C, de Sousa Junior W C. 2017. Comparison of two bias correction methods for precipitation simulated with a regional climate model. Theor Appl Climatol, 127: 841–852
van der Wiel K, Kapnick S B, Vecchi G A, Smith J A, Milly P C D, Jia L. 2018. 100-year lower Mississippi floods in a global climate model: Characteristics and future changes. J Hydrometeorol, 19: 1547–1563
Viglione A, Merz R, Salinas J L, Blöschl G. 2013. Flood frequency hydrology: 3. A Bayesian analysis. Water Resour Res, 49: 675–692
Vormoor K, Lawrence D, Heistermann M, Bronstert A. 2015. Climate change impacts on the seasonality and generation processes of floods-projections and uncertainties for catchments with mixed snowmelt/rainfall regimes. Hydrol Earth Syst Sci, 19: 913–931
Wang J, Yang B, Qin C, Kang S, He M, Wang Z. 2014. Tree-ring inferred annual mean temperature variations on the southeastern Qinghai-Xizang during the last millennium and their relationships with the Atlantic Multidecadal Oscillation. Clim Dyn, 43: 627–640
Wang Q, Huang A, Zhao Y, Zhou Y, Yang B, Zhang L, Wu H, Jiang Y, Kan M. 2016. Evaluation of the precipitation seasonal variation over eastern China simulated by BCC_CSM model with two horizontal resolutions. J Geophys Res Atmos, 121: 8374–8389
Wang S W. 2010. The medieval warm period and the little ice age (in Chinese). Adv Clim Change Res, 6: 388–390
Wang S W, Wang R S. 1991. Little ice-age in China. Chin Sci Bull, 36: 217–220
Xiao D M, Qin N S, Huang X M. 2016. A 412-year March-May precipitation series reconstructed from tree-ring records in the source regions of the Yangtze River (in Chinese). J Glaciol Geocryol, 38: 1691–1700
Xu H F, Zhang H, Chen F, Chen Y P. 2020. Precipitation reconstruction for upper reaches of Bailong River by Pinus tabulaeformis tree-ring and its hydrological significance (in Chinese). Yangtze River, 51: 64–70
Xu X N. 2015. The impact of climate change and human activities on water discharge and sediment load entering Poyang Lake Basin (in Chinese). Dissertation for Doctoral Degree. Nanjing: Nanjing University. 1–56
Yang X, Magnusson J, Huang S, Beldring S, Xu C Y. 2020. Dependence of regionalization methods on the complexity of hydrological models in multiple climatic regions. J Hydrol, 582: 124357
Zeng Q, Chen H, Xu C Y, Jie M X, Hou Y K. 2016. Feasibility and uncertainty of using conceptual rainfall-runoff models in design flood estimation. Hydrol Res, 47: 701–717
Zha X C, Huang C C, Pang J L, Ji L, Wang G P. 2017. The palaeoflood events recorded by slackwater deposits in sedimentary profiles during the Eastern Han Dynasty in the upper reaches of the Hanjiang River (in Chinese). Acta Geogr Sin, 72: 96–106
Zhang L, Dong M, Wu T. 2011. Changes in precipitation extremes over Eastern China simulated by the Beijing climate center climate system model (BCC_CSM1.0). Clim Res, 50: 227–245
Zhang Q, Chen J, Becker S. 2007. Flood/drought change of last millennium in the Yangtze Delta and its possible connections with Tibetan climatic changes. Glob Planet Change, 57: 213–221
Zhang S, Chen J, Gu L. 2021. Overall uncertainty of climate change impacts on watershed hydrology in China. Intl J Climatol, 42: 507–520
Zhao R J. 1992. The Xinanjiang model applied in China. J Hydrol, 135: 371–381
Zhou L, Shi Y, Zhao Y Q, Yang Y, Jia J J, Gao J H, Wang Y P, Li Z H, Zhang Y Z, Guo Y Q, Shi B W, Gao S. 2021. Extreme floods of the Changjiang River over the past two millennia: Contributions of climate change and human activity. Mar Geol, 433: 106418

(Responsible editor: Bao YANG)